Transportation Research Part C xxx (xxxx) xxx

Contents lists available at ScienceDirect

Transportation Research Part C

journal homepage: www.elsevier.com/locate/trc

Disturbances and safety analysis of linear adaptive cruise control for cut-in scenarios: A theoretical framework

Zihao Li [a], Yang Zhou [a,*], Danjue Chen [b], Yunlong Zhang [a]

[a] Zachry Department of Civil & Environmental Engineering, Texas A&M University, College Station, TX 77843 United States
[b] Department of Civil, Construction, and Environmental Engineering, North Carolina State University, NC 27695 United States

ARTICLE INFO

Keywords:
Automated vehicle (AV)
Disturbance analysis
Adaptive cruise control (ACC)
Cut-in scenario
Theoretical Analysis

ABSTRACT

Although adaptive cruise control (ACC) has been widely analyzed in the car-following process, the way it reacts to cut-in maneuvers has been largely ignored. The cut-in maneuvers may trigger multiple disturbances to traffic, resulting in traffic oscillations and corresponding rear-end crashes. Hence, this study provides a theoretical analysis framework to model the disturbance evolution for ACC under cut-in scenarios. Specifically, we first derive the general ACC dynamic evolution based on the widely adopted ACC (i.e., linear feedback control) by applying Caley-Hamilton theorem. Given that, two representative cut-in scenarios are designed to comprehensively understand the impact of cut-in vehicle behavior as well as control parameters on the safety and stability of the ACC system. Enable by the interpretability nature of ACC dynamic analytical solution, necessary and sufficient conditions for overshoot and potential safety risks are derived. The proposed framework is further applied to analyze the cut-in disturbance evolution of commercial ACC systems using field-test data and calibrated control parameters, by which the probabilistic safety and stability condition is provided. Through the above efforts, the framework is instrumental in robust ACC design under cut-in scenarios.

1. Introduction

Adaptive cruise control (ACC) serves as the fundamental vehicular automation function to maintain a desired spacing from immediately preceding vehicle, which brings promises to enhance traffic safety and efficiency (Li et al., 2017; Zhou et al., 2019). There exist three major ACC system categories: linear control (Naus et al., 2010; Wang et al., 2020b; H. Zhou et al., 2022), optimal control (Wang et al., 2020a; Zhou et al., 2019, 2017), and reinforcement learning based controller (Cheng et al., 2019; Shi et al., 2021). Regardless of the control logic and algorithm, one of the essential properties of the ACC design is the robustness against various disturbances (e.g., temporary velocity drops and merging/diverging flow) to ensure safety and stability. Previous studies (Li et al., 2023; Montanino and Punzo, 2021; Ploeg et al., 2014; Zhou et al., 2022a; Zhou et al., 2017) have conducted rigorous mathematical derivation to guarantee the local and string stability of linear control through proper selection of control parameters, which assures the disturbance dissipates as time goes to infinity and will not be amplified through the following vehicle and vehicular string respectively. Besides, the string stability have also been proven for nonlinear control (e.g., Model Predictive Control, MPC), as well as in scenarios incorporating delays and heterogenous traffic flow (Liu et al., 2001; Montanino and Punzo, 2021; Ward, 2009; Zhou et al., 2019). These approaches guarantee the desired local-stable and string-stable vehicle behavior, which helps in dampening traffic oscillations.

* Corresponding author.
E-mail address: yangzhou295@tamu.edu (Y. Zhou).

https://doi.org/10.1016/j.trc.2024.104576
Received 15 January 2024; Accepted 18 March 2024
Available online 28 March 2024

In the traditional stability analysis, they typically assume that the system is in equilibrium, but this assumption does not hold when an initial disturbance (e.g., cut-in disturbance) is introduced. Therefore, the stability is insufficient in fully describing the evolution of ACC's dynamic over time and the corresponding potential collision risk (Khound et al., 2021; Li, 2022). ACC stability as well as safety, while interrelated, are not equivalent, though a stable ACC is generally safer than an unstable one. Stability describes properties guaranteeing disturbance resolving and dampening but fails to depict the 'in-process' disturbance. Whereas, during the disturbance resolving and dampening, the transitional dynamics of a stable ACC system can also create voids as well as cause collisions. In the control theory, a phenomenon wherein the system's response to external disturbance either exceeds or fails short of its equilibrium, is referred to as positive or negative overshoot (Nise, 2020). In the spacing response of the ACC system, positive overshoot causes the spacing between two vehicles to exceed the ideal following spacing than necessary, which causes traffic void and reduces traffic throughput (Chen et al., 2020). On the other hand, the negative overshoot results in an undesirably reduced spacing. If the magnitude of the negative overshoot exceeds safety thresholds, the risk of rear-end collisions significantly increases (Jayasuriya and Dharne, 2002). It is, therefore, of paramount importance to distinguish between stability, which pertains primarily to the system's inherent capacity to regain equilibrium, and safety, which encompasses the entire evolution of the ACC system toward its equilibrium amidst various disturbances.

Current disturbance analysis primarily pertains to a pure car-following process in both theoretical and practical aspects (Gunter et al., 2021; Li and Shrivastava, 2002; Marsden et al., 2001; Ossen and Hoogendoorn, 2011). Different from a pure car-following process, the cut-in vehicles will simultaneously trigger the disturbance by introducing target spacing deviation and speed changes of the following vehicle. Besides, the cut-in vehicle itself may accelerate or decelerate to reach its car-following steady states, which further contributes to traffic oscillations (Ahn and Cassidy, 2007; Zheng et al., 2013) and corresponding rear-end collision (Li et al., 2017; Zheng et al., 2010). Addressing these disturbances has led to several studies proposing advanced controls, such as learning-based stochastic MPC (Kazemi et al., 2018), control mode transition (Milanés and Shladover, 2016), and adaptive control (Bang and Ahn, 2018). However, commercial ACC system predominantly adopt linear control, which may not effectively handle cut-in disturbances, potentially leading to safety risk and overshoot condition (Li et al., 2021; Shi and Li, 2021). Despite the notable progress in control approaches, understanding of disturbance evolution subject to cut-in maneuver for linear ACC is significant but remains elusive (Li et al., 2021).

The evolution of cut-in disturbance in the linear ACC system is a multifaceted process, influenced by multiple factors. The selection of control gain directly influences the acceleration profile of the controlled vehicle. Furthermore, the acceleration/deceleration boundaries of the ACC system have concurrent effects on ACC behavior and response characteristics. When the cut-in vehicle has merged into target lane, the speed oscillation further introduces disturbances in ACC evolution. It is evident that ACC design and the behavior of cut-in vehicle are both critical factors in ACC dynamic evolution, yet their compounded effects on safety and overshoot of the ACC system, along with their resultant implications (e.g., potential collision or traffic void), remain inadequately studied. Some relevant studies on ACC disturbance analysis under cut-in scenarios have been conducted. Chen et al. (2020) analytically investigated the impact mechanism of heterogeneity in driving behavior (i.e., preferred acceleration and car-following behavior) under lane-changing in mixed traffic flow. However, the study simplified the ACC preferred acceleration setting (i.e., larger or smaller acceleration than HDV) and mainly focused on traffic throughput, rather than safety. Other related studies (Makridis et al., 2021; Zhao et al., 2019) resorting to field experiment-based approaches have demonstrated that abnormal cut-in maneuvers (i.e., over-aggressive and over-conservative) can result in safety–critical situations. Despite these findings, it should be noted that such method lacks the capability to directly analyze and interpret the disturbance evolution as well as potential safety risk caused by the combined impact of cut-in vehicle behaviors and ACC design. Therefore, it is imminent to build up a fine-grained and firm understanding of ACC dynamic evolution under cut-in scenarios and its corresponding safety.

To bridge these research gaps in cut-in disturbance analysis, this study provides a theoretical and analytical framework of disturbances evolution and potential safety risks for linear ACC under cut-in scenarios. We theoretically examine two critical issues: (i) The manifestation of ACC dynamic evolution in response to cut-in disturbances, a process significantly impacted by ACC design (i.e., different control parameters) and cut-in behavior (i.e., initial cut-in condition and velocity change); and (ii) the impact of ACC dynamic evolution on the safety of vehicle subjected to cut-in maneuvers. We first provide an analytic derivation of ACC dynamic evolution by applying the Caley-Hamilton theorem, assuming a widely adopted ACC system based on second-order linear feedback control. Furthermore, the necessary and sufficient conditions for the ACC system's inherent oscillation and the engagement of nonlinear control law are derived, enabled by the interpretability nature of ACC state analytical solution. Two specific cut-in scenarios are designed to provide a comprehensive understanding on the impact of cut-in vehicle behavior (i.e., cut-in position and speed and acceleration/deceleration behavior after cut-in) as well as control parameters on the overshoot and safety condition of the ACC system. The proposed analysis framework is further applied to analyze dynamic evolution of commercial ACCs under cut-in disturbances, using field-test data (Li et al., 2022) and corresponding calibration results (Y. Zhou et al., 2022), by which the probabilistic overshoot and safety condition of commercial ACCs is provided. The major contribution of this study is our focus on the disturbance evolution in linear ACC systems under cut-in maneuvers, addressing the limitations of existing local/string stability analysis and aiming to ensure both stability and safety simultaneously.

In this study, we focus on linear ACC system (i.e., linear feedback control) because (i) its wide use in commercial ACC systems; (ii) its ability to provide foundational insights into ACC dynamics, essential for understanding more complex systems; and (iii) the theoretical analysis challenges posed by the implicit control laws of nonlinear control. Insights from this study are crucial for enhancing the robustness of linear ACC systems against cut-in disturbances. There are two notable limitations of linear feedback control: time-invariant control parameters and the inability to integrate collision-free constraints (Zhou et al., 2017). By analyzing the safety and overshoot conditions of linear ACC systems with acceleration/deceleration boundaries, we can explore the relationship

between cut-in maneuvers, ACC parameters, and safety/overshoot conditions. This relationship offers insights into making driving decisions, such as whether to overtake or yield, in response to a cut-in maneuver. It could also derive a feasible region of control gains to ensure stability and safety, given a cut-in maneuver. This complements the limitations of local/string stability analysis in linear feedback control by incorporating disturbance and safety analysis.

The remainder of the paper is organized as follows: Section 2 presents the general derivation framework for ACC dynamic evolution under cut-in disturbances, and Section 3 provides scenarios-based derivation and analysis by giving velocity profiles of cut-in vehicle. Section 4 conducts a series of numerical experiments to understand ACC evolution and investigate related factors, as well as evaluate the probabilistic performance of field-testing ACC systems under cut-in maneuvers. Finally, the conclusion and future research are outlined in Section 5.

2. General derivation framework for ACC traffic dynamics evolution

As suggested by Chen et al. (2020) and Liu et al. (2021), current ACC algorithms in the market are predominantly linear feedback controllers. Hence, a linear controller with second-order dynamics is adopted in our paper for the following analysis, and it can be further extended to incorporate a higher-order dynamics ACC controller or nonlinear ACC controller that can be approximated through linearization. This section first derived ACC dynamic evolution under cut-in scenarios adopting the Caley-Hamilton theorem. Then, by considering the primary nonlinearity of the ACC system, i.e., bounded acceleration/deceleration, the general framework for ACC dynamic evolution is developed. These ACC dynamics evolution will serve as the base for the disturbance analysis and safety risks identification.

In detail, by defining the system state for vehicle i at time interval t following $x_i(t) = [\Delta d_i(t), \Delta v_i(t)]^T$. $\Delta d_i(t) = d_i(t) - d_i^*(t)$ represents the deviation of the spacing $d_i(t)$ between vehicle i and $i-1$ at time interval t and the ideal spacing $d_i^*(t) = v_i(t) \bullet \tau^* + \delta^*$, in which τ^* and δ^* are the pre-defined constant time gap and standstill distance, respectively. $\Delta v_i(t) = v_{i-1}(t) - v_i(t)$ is the velocity difference between preceding and following vehicle. Vehicular dynamics together can be formulated as a linear time-invariant (LTI) system as below:

$$\dot{x}_i(t) = Ax_i(t) + Bu_i(t) + Da_{i-1}(t) \tag{1}$$

Where the $A = \begin{bmatrix} 0 & 1 \\ 0 & 0 \end{bmatrix}, B = \begin{bmatrix} -\tau^* \\ -1 \end{bmatrix}, D = \begin{bmatrix} 0 \\ 1 \end{bmatrix}. u_i(t) = a_i(t)$ represents the control input, the acceleration for vehicle i. $a_{i-1}(t)$ is acceleration for preceding vehicle $i-1$.

According to the linear feedback law, we can have:

$$u_i(t) = kx_i(t) \tag{2}$$

Where $k = [k_s, k_v]$ are the feedback gain for the deviation from equilibrium spacing $\Delta d_i(t)$ and speed difference $\Delta v_i(t)$, respectively. By combining Eq. (1) and (2), Eq. (3) can be obtained as:

$$\dot{x}_i(t) = A_d x_i(t) + D_d a_{i-1}(t) \tag{3}$$

$$A_d = \begin{bmatrix} -\tau^* k_s & 1 - \tau^* k_v \\ -k_s & -k_v \end{bmatrix}, D_d = \begin{bmatrix} 0 \\ 1 \end{bmatrix}$$

Eq. (3) is also an LTI system, and its continuous solution can be solved by taking integral on both hand sides, which finally renders:

$$x_i(t) = \underbrace{e^{A_d(t-t_0)} x_i(t_0)}_{free response} + \underbrace{\int_{t_0}^{t} e^{A_d(t-\varphi)} D_d a_{i-1}(\varphi) d\varphi}_{forced response} \tag{4}$$

In Eq. (4), $x_i(t)$ contains two components, including free response and forced response, where the free response describes how ACC reacts to initial conditions of cut-in vehicles $x_i(t_0)$, and the forced response represents the further behaviors contributed by cut-in vehicle's acceleration and deceleration after cut-in. In both responses, the matrix exponential $e^{A_d t}$ can be obtained by Taylor-series expansion $e^{A_d t} = I + A_d t + \frac{1}{2!}(A_d t)^2 + \frac{1}{3!}(A_d t)^3 + \cdots$, but it greatly prohibits the tractability and interpretability. To make Eq. (4) more interpretable, a further technique is needed to simplify $e^{A_d t}$. Note that simplifying $e^{A_d t}$ is non-trivial since matrix A_d is non-diagonal nor nilpotent. Therefore, we apply the Cayley-Hamilton theorem (Straubing, 1983), as presented in **Appendix 1**.

Proposition 1. (*When* $(\tau^* k_{si} + k_{vi})^2 - 4k_{si} \geq 0$, *the eigenvalues of* A_d *are all real numbers, and*)

$$e^{A_d t} = \alpha_0 I + \alpha_1 A_d = \begin{bmatrix} e^{\lambda_1 t} - \frac{e^{\lambda_1 t} - e^{\lambda_2 t}}{\lambda_1 - \lambda_2}(\lambda_1 + \tau^* k_s) & \frac{e^{\lambda_1 t} - e^{\lambda_2 t}}{\lambda_1 - \lambda_2}(1 - \tau^* k_v) \\ -\frac{e^{\lambda_1 t} - e^{\lambda_2 t}}{\lambda_1 - \lambda_2} k_s & e^{\lambda_1 t} - \frac{e^{\lambda_1 t} - e^{\lambda_2 t}}{\lambda_1 - \lambda_2}(\lambda_1 + k_v) \end{bmatrix} \tag{5}$$

Where $\lambda_1 = \frac{-(\tau^* k_s + k_v) + \sqrt{(\tau^* k_s + k_v)^2 - 4k_s}}{2}$ and $\lambda_2 = \frac{-(\tau^* k_s + k_v) - \sqrt{(\tau^* k_s + k_v)^2 - 4k_s}}{2}$

Because $e^{\lambda_1 t}$ and $e^{\lambda_2 t}$ are monotonic functions, the ACC itself should be a non-oscillatory system resulting in smooth ACC dynamic evolution without overshoot. When $\lambda_1, \lambda_2 < 0$, smaller eigenvalues correspond to faster convergence towards equilibrium, because the magnitude of the eigenvalues determines the speed at which the system's response decays over time.

Proposition 2. (*When* $(\tau^* k_s + k_v)^2 - 4k_s < 0$, *the eigenvalues of* A_d *have an imaginary part, and*)

$$e^{A_d t} = \alpha_0 I + \alpha_1 A_d = \begin{bmatrix} e^{zt}\cos yt - \dfrac{e^{zt}(\tau^* k_s - z)}{y}\sin yt & \dfrac{e^{zt}(1 - \tau^* k_v)}{y}\sin yt \\ \dfrac{-k_s e^{zt}}{y}\sin yt & e^{zt}\cos yt - \dfrac{e^{zt}(k_v - z)}{y}\sin yt \end{bmatrix} \tag{6}$$

Where $z = -\frac{1}{2}(\tau^* k_s + k_v)$ and $y = \frac{1}{2}\left(\sqrt{(\tau^* k_s + k_v)^2 - 4k_s}\right)$.

The detailed proofs of **Propositions 1 and 2** are provided in **Appendix 2**. As can be found from Proposition 1 and 2, the eigenvalues of A_d in ACC system, λ_1, λ_2 plays crucial roles in determining the system's stability and response characteristics, including whether the system is oscillatory or non-oscillatory (Franklin et al., 2002). If all the eigenvalues have a negative real part, the ACC system is locally stable. In the case of oscillatory systems, the eigenvalues have complex conjugates paired with negative real parts, which results in oscillatory behavior in the system's response due to the sinusoidal/cosinusoidal terms. Moreover, the y determines the frequency of system oscillation, and the oscillation magnitudes decay exponentially by z. Note that the oscillatory behavior of the ACC system itself is independent of local/string instability. As long as the oscillations, attributable to the ACC design itself, exhibit decaying magnitude, the ACC system is stable.

Remark 1. (.) $e^{A_d t}$ of the second-order vehicle dynamics can be derived analytically. For higher-order vehicle dynamics, such as third-order dynamics (Zhou et al., 2020), or dynamics with delay (Brunner et al., 2022), $e^{A_d t}$ can be approximated by Taylor expansion. Since it is not the main focus of our paper, we stick to the second-order vehicle dynamics for the following analysis.

By combining Proposition 1 or Proposition 2, the preliminary solution of system state $x_i(t)$ can be obtained in Eq. (4). To further incorporate the impact of nonlinearity, such as bounded acceleration/deceleration, we derived the ACC dynamic evolution based on Eq. (4). Since integration by pieces always holds, Eq. (4) can be further expanded by conditioning on time t that acceleration/deceleration boundary that is not touched as Proposition 3.

Proposition 3. Given $k_s, k_v, \tau^*, u_b, a_{i-1}(t), \Delta d_i(t_0), \Delta v_i(t_0)$, and t_0, if the below equation on t has a positive solution, the ACC system will show nonlinear behavior due to the bounded acceleration/deceleration. Otherwise, the ACC system follows linear feedback control law as Eq. (4) with **Propositions 1** or **2**.

$$[k_s \quad k_s(t - t_0) + k_v]\begin{bmatrix}\Delta d_i(t_0) \\ \Delta v_i(t_0)\end{bmatrix} + [k_s \quad k_v]\begin{bmatrix} -\dfrac{t^2}{2} + (t_0 - \tau^*)t + \tau^* t_0 - \dfrac{t_0^2}{2} \\ -t + t_0 \end{bmatrix} u_b + \underbrace{\int_{t_0}^{t} (k_s(t - \varphi) + k_v)a_{i-1}(\varphi)d\varphi}_{forcedresponse} - u_b = 0 \tag{7}$$

Proof. Based on Eq. (1) and bounded acceleration/deceleration, the analytical solution to the continuous ACC system can be obtained:

$$x_i(t) = e^{A(t-t_0)}x_i(t_0) + \int_{t_0}^{t} e^{A(t-\varphi)}Bu_b d\varphi + \int_{t_0}^{t} e^{A(t-\varphi)}Da_{i-1}(\varphi)d\varphi \tag{8-a}$$

$$u_b = \begin{cases} u_{\min} kx_i(t) \le u_{\min} \\ u_{\max} kx_i(t) \ge u_{\max} \end{cases} \tag{8-b}$$

A is a nilpotent matrix since its square results in a zero matrix, which allows for simplifying the Taylor expansion. $e^{A(t-t_0)} = I + A(t - t_0) = \begin{bmatrix} 1 & t - t_0 \\ 0 & 1 \end{bmatrix}$, and u_b is the bounded acceleration or deceleration. From Eq. (2) and (8), we can have Eq. (7). By analyzing the solution of Eq. (7), Proposition 3 can be obtained. Taking $a_{i-1}(\varphi) = 0$ (i.e., constant cut-in velocity) as an example, Eq. (7) could be revised as below:

$$u_b = kx_i(t) = [k_s \quad k_s t + k_v]\begin{bmatrix}\Delta d_i(0) \\ \Delta v_i(0)\end{bmatrix} + [k_s \quad k_v]\begin{bmatrix} -\dfrac{t^2}{2} - \tau^* t \\ -t \end{bmatrix} u_b \tag{9-a}$$

Eq. (9-a) can be further simplified to Eq. (9-b), for which a solution can be readily derived as a quadratic equation of t.

$$-\frac{k_s u_b}{2}t^2+(k_s\Delta v_i(0)-k_s u_b\tau^*-k_v u_b)t+k_s\Delta d_i(0)+k_v\Delta v_i(0)-u_b=0 \tag{9-b}$$

The specific nonlinearity interval for ACC system is given in the following scenario-based derivation. If $a_{i-1}(\varphi)$ is the piecewise function (i.e., non-integrable), the definite integral of forced response can be obtained separately by each interval, and the framework remains valid. Moreover, Proposition 3 remains applicable for deriving the nonlinearity interval of the ACC system, even in cases where acceleration/deceleration of cut-in vehicles (i.e., $a_{i-1}(\varphi)$) exceeds or falls below the boundary.

3. Scenarios-based Derivation and Analysis Framework

To further understand the disturbance evolution impacted by ACC design and cut-in vehicles' behaviors, we conduct scenarios-based derivation and analysis by different cut-in vehicles' initial condition $x_i(t_0)$ and the cut-in vehicle's acceleration/deceleration behavior $a_{i-1}(\varphi)$. In **Scenario 1**, the cut-in vehicle triggers the initial disturbance (i.e.,$x_i(t_0)\neq 0$) while maintaining a constant speed afterward (i.e., $a_{i-1}(\varphi)=0$). Based on **Scenario 1**, we further assume the behaviors of the cut-in vehicle after cut-in by exemplar **Scenario 2** as shown in Eq. (10) and Fig. 1. In **Scenario 2**, state evolution of the ACC system is jointly impacted by initial cut-in condition and the behaviors of the cut-in vehicle, which means ACC system has both free and forced responses. According to the analytic formulation of $e^{A_d t}$ and given velocity profiles from the cut-in vehicle, we can derive the specific solution of Eq. (4), which is the dynamic evolution of the ACC system under disturbance. Note that the designed ACC system may behave distinctly due to the difference of A_d, the analytical solution for ACC state evolution is respectively provided to understand the overshoot and safety condition under two specific scenarios with **Propositions 1 and 2**.

$$a_{i-1}(\varphi)=\begin{cases} a_1 t\in(0,t_1) \\ a_2 t\in(t_1,t_2) \\ 0 others \end{cases} \tag{10}$$

In this study, we define safety risk as the bumper-to-bumper distance of two vehicles (i.e., following and cut-in vehicles) less than a pre-defined threshold (ε). As to the overshoot, if the extremum of $\Delta d_i(t)$ exists, and its sign is different from the initial state $\Delta d_i(t_0)$, it indicates the overshoot in spacing response exists. Depending on the sign of $\Delta d_i(t_0)$, it can be further categorized as positive overshoot and negative overshoot, illustrated by Fig. 2**(a)** and Fig. 2**(b)**, respectively. As demonstrated in Fig. 2**(a)**, the initial bumper-to-bumper distance is less than equilibrium (i.e., negative spacing deviation). Both non-oscillatory (blue profile) and oscillatory (red profile) ACC systems will gradually converge to equilibrium, but the oscillatory ACC system inherently exhibits decay oscillation due to the control parameters setting. This oscillation results in positive overshoot, as the response exceeds the equilibrium (red profile). Positive overshoot will create voids in traffic streams due to large spacing, which reduces traffic throughput. Additionally, collisions may happen if the initial cut-in spacing is excessively small (yellow profile) or due to the impact of bounded acceleration/deceleration in the ACC system (green profile), even in the absence of an overshoot. Conversely, as shown by Fig. 2**(b)**, the initial spacing deviation is positive. The negative overshoot will occur when the response spacing falls below equilibrium. Negative overshoot causes spacing to be small, which may result in near-collision or collision conditions (red and green profiles). ACC system reaching the equilibrium spacing gradually in a safe manner, as shown by the blue profiles in Fig. 2, is more desirable. Note that both oscillatory and non-oscillatory ACC systems are locally stable, and the non-oscillatory ACC system does not correspond to string stability. It is because the local/string stability is the inherent property of ACC design, while the non-oscillation in ACC dynamic evolution is related to both ACC system design and external disturbance, as oscillation can originate from the ACC system itself or from the cut-in vehicle.

3.1. Derivation of Scenario 1 under non-oscillatory ACC system

Under Scenario 1, the ACC system solely has a free response, which is the reaction to the initial cut-in condition. Given the initial condition $x_i(t_0)$, when vehicle just cut-in and $a_{i-1}(\varphi)\equiv 0$, the state evolution of ACC can be derived from Eq. (5) as Eq. (14) if

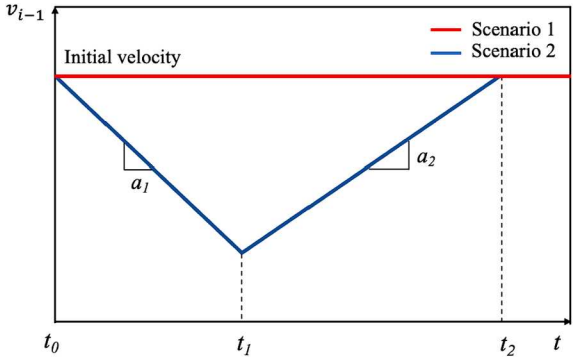

Fig. 1. Speed profile for Scenario 1 and 2.

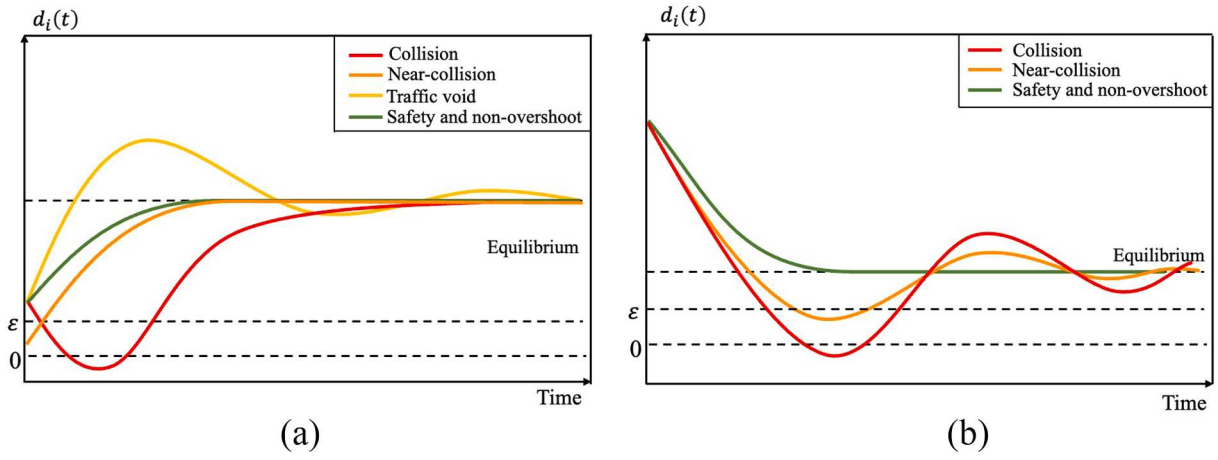

Fig. 2. Illustration of overshoot and safety risk for the ACC system (a) positive overshoot; (b) negative overshoot.

Propositions 1 and 3 hold. Based on Eq. (11), the overshoot and safety risk conditions can be derived from **Propositions 4 and 5**.

$$\begin{bmatrix} \Delta d_i(t) \\ \Delta v_i(t) \end{bmatrix} = \begin{cases} \begin{bmatrix} 1 & t \\ 0 & 1 \end{bmatrix} \begin{bmatrix} \Delta d_i(0) \\ \Delta v_i(0) \end{bmatrix} + \begin{bmatrix} -\frac{t^2}{2} - \tau^* t \\ -t \end{bmatrix} u_b t \in [0, t_w] \\ M(t, t_w) \begin{bmatrix} \Delta d_i(t_w) \\ \Delta v_i(t_w) \end{bmatrix} t \in (t_w, \infty) \end{cases} \tag{11}$$

ACC reaches bounded acceleration/deceleration in $T_w = [0, t_w]$. Suppose ACC follows linear feedback control law, then $t_w = 0$. Besides, $\mathcal{M}(t, t_0) = \begin{bmatrix} e^{\lambda_1(t-t_0)} - \frac{e^{\lambda_1(t-t_0)} - e^{\lambda_2(t-t_0)}}{\lambda_1 - \lambda_2}(\lambda_1 + \tau^* k_s) & \frac{e^{\lambda_1(t-t_0)} - e^{\lambda_2(t-t_0)}}{\lambda_1 - \lambda_2}(1 - \tau^* k_v) \\ -\frac{e^{\lambda_1(t-t_0)} - e^{\lambda_2(t-t_0)}}{\lambda_1 - \lambda_2} k_s & e^{\lambda_1(t-t_0)} - \frac{e^{\lambda_1(t-t_0)} - e^{\lambda_2(t-t_0)}}{\lambda_1 - \lambda_2}(\lambda_1 + k_v) \end{bmatrix}$ represents a function of free response under non-oscillatory system that mapping $x_i(t_0)$ to $x_i(t)$.

Lemma 1. **(Switch time):** Nonlinear interval is $T_w = [0, t_w]$, where switch time from nonlinear behavior due to bounded acceleration/deceleration to linear feedback control law is given by $t_w = \max\left(\frac{-B \pm \sqrt{D}}{2A}\right)$. When $D = B^2 - 4AC < 0$ or $\max\left(\frac{-B \pm \sqrt{D}}{2A}\right) \leq 0$, the ACC system adheres strictly to the linear control law and $t_w = 0$, where $A = -\frac{k_s u_b}{2}, B = k_s \Delta v_i(0) - k_s u_b \tau^* - k_v u_b$, and $C = k_s \Delta d_i(0) + k_v \Delta v_i(0) - u_b$. The proof can be found in **Appendix 3**.

Proposition 4. **(Overshoot condition):** When ACC exhibits nonlinear behavior, the spacing overshoot exists if Eq. (12-a) and $t^*_{\Delta d,n} \leq t_w$ or Eq. (12-b) and $t^*_{\Delta d,n} > t_w$ are satisfied, where $t^*_{\Delta d,n} = \frac{\Delta v_i(0) - u_b \tau^*}{u_b}$.

$$\Delta d_i\left(t^*_{\Delta d,n}\right) \bullet \Delta d_i(0) < 0 \tag{12-a}$$

$$\Delta d_i(t_w) \bullet \Delta d_i(0) < 0 \tag{12-b}$$

Proof. From Eq. (11), the spacing response under **Scenario 1** can be given as:

$$\Delta d_i(t) = \begin{cases} \Delta d_i(0) + \Delta v_i(0) t - \frac{u_b t^2}{2} - u_b \tau^* t t \in [0, t_w] \\ e^{\lambda_1(t-t_w)} \Delta d_i(t_w) - \frac{e^{\lambda_1(t-t_w)} - e^{\lambda_2(t-t_w)}}{\lambda_1 - \lambda_2}(\lambda_1 + \tau^* k_s) \Delta d_i(t_w) + \frac{e^{\lambda_1(t-t_w)} - e^{\lambda_2(t-t_w)}}{\lambda_1 - \lambda_2}(1 - \tau^* k_v) \Delta v_i(t_w) t \in (t_w, \infty) \end{cases} \tag{13-a}$$

According to the definition of overshoot, the extremum of Eq. (13-a) should exist, and its sign should be different from $\Delta d_i(0)$. Then, we can set $\Delta d_i(t)' = 0$, and derive the time of extreme spacing response (t^*), as below:

$$\begin{cases} t^*_{\Delta d,n} = \dfrac{\Delta v_i(0) - u_b\tau^*}{u_b} \\ t^*_{\Delta d,l} = \dfrac{\ln\dfrac{-N}{M}}{\lambda_1 - \lambda_2} + t_w \end{cases} \tag{13-b}$$

Where $M = \lambda_1(-\lambda_2 - \tau^* k_s)\Delta d_i(0) + \lambda_1(1 - \tau^* k_v)\Delta v_i(0)$ and $N = \lambda_2(\lambda_1 + \tau^* k_s)\Delta d_i(0) - \lambda_2(1 - \tau^* k_v)\Delta v_i(0)$

Therefore, Proposition 4 and Lemma 2 can be obtained considering the asymptotic stability nature of a stable ACC system. Based on the signs of $\Delta d_i(0)$, we can further distinguish the positive and negative overshoot following Remark 2.

Lemma 2. **(Overshoot condition)**: When the ACC system follows linear control law ($t_w = 0$), the overshoot of the spacing response happens if Eq. (14-a) and (14-b) are satisfied.

$$-\frac{N}{M} > 0 \tag{14-a}$$

$$\Delta d_i\left(t^*_{\Delta d,l}\right) \bullet \Delta d_i(0) < 0 \tag{14-b}$$

Remark 2. If **Proposition 4** or **Lemma 2** holds and $\Delta d_i(0) < 0$, the positive overshoot happens. Conversely, if $\Delta d_i(0) > 0$, the negative overshoot happens. The illustration has shown in **Fig. 2**.

Proposition 5. **(Safety risk condition)**: When the following inequality equations are satisfied, the ACC system with nonlinearity property has safety risk. Specifically, when $\varepsilon = 0$, crashes happen.

If $t^*_{d,n} \notin [0, t_w]$,

$$\min(d_i(0),\ d_i(t_w)) \le \varepsilon \tag{15-a}$$

If $t^*_{d,n} \in [0, t_w]$,

$$\min\left(d_i(0),\ d_i\left(t^*_{d,n}\right)\right) \le \varepsilon \tag{15-b}$$

Proof. According to the definition of the safety risk, we can have the safety risk condition:

$$d_i(t) = \Delta d_i(t) + (v_{i-1}(t) - \Delta v_i(t))\tau^* \le \varepsilon \tag{16-a}$$

By substituting Eq. (13-a) into Eq. (16-a), we can have:

$$d_i(t) = \begin{cases} -\dfrac{u_b t^2}{2} + \Delta v_i(0)t + \tau^* v_{i-1}(t) + \Delta d_i(0) - \tau^* \Delta v_i(0) t \in [0, t_w] \\ \dfrac{e^{\lambda_1(t-t_w)}}{\lambda_1 - \lambda_2}[-\lambda_2 \Delta d_i(t_w) + (1 + \tau^*\lambda_2)\Delta v_i(t_w)] + \dfrac{e^{\lambda_2(t-t_w)}}{\lambda_1 - \lambda_2}[\lambda_1 \Delta d_i(t_w) - (1 + \lambda_1\tau^*)\Delta v_i(t_w)] + v_{i-1}(t)\tau^* t \in (t_w, \infty) \end{cases} \tag{16-b}$$

$v_{i-1}(t)$ in **Scenario 1** is constant, then Eq. (16-b) can be simplified as:

$$d_i(t) = \begin{cases} -\dfrac{u_b t^2}{2} + \Delta v_i(0)t + \tau^* v_{i-1}(0) + \Delta d_i(0) - \tau^* \Delta v_i(0) t \in [0, t_w] \\ Ae^{\lambda_1(t-t_w)} + Be^{\lambda_2(t-t_w)} + Ct \in (t_w, \infty) \end{cases} \tag{16-c}$$

Where $= \frac{-\lambda_2 \Delta d_i(t_w) + (1+\lambda_2\tau^*)\Delta v_i(t_w)}{\lambda_1 - \lambda_2}$, $B = \frac{\lambda_1 \Delta d_i(t_w) - (1+\lambda_1\tau^*)\Delta v_i(t_w)}{\lambda_1 - \lambda_2}$, and $C = v_{i-1}(0)\tau^*$. By derivatizing Eq.(16-c) with respect to t, the extremum of two pieces in Eq. (16-c) can be obtained:

$$\begin{cases} t^*_{d,n} = \dfrac{\Delta v_i(0)}{u_b} \\ t^*_{d,l} = \dfrac{\ln\left(-\dfrac{\lambda_1 A}{\lambda_2 B}\right)}{\lambda_1 - \lambda_2} + t_w \end{cases} \tag{16-d}$$

To satisfy Eq. (16-a), **Proposition 5** and Lemma 3 can be given by comparing the states of the extremum moment, switch moment, and initial cut-in.

Lemma 3. **(Safety risk condition)**: The ACC system following linear control law ($t_w = 0$) is subject to the safety risk, when Eq. (16-e) is satisfied.

$$\min\left(d_i(0),\, d_i\left(t_{d,l}^{*}\right)\right) \le \varepsilon \tag{16-e}$$

3.2. Derivation of Scenario 1 under oscillatory ACC system

When Proposition 2 holds, the ACC system itself has oscillatory behavior, so the state evolution of ACC can be derived from Eq. (6) as Eq. (17) considering Proposition 3.

$$\begin{bmatrix}\Delta d_i(t)\\ \Delta v_i(t)\end{bmatrix} = \begin{cases}\begin{bmatrix}1 & t\\ 0 & 1\end{bmatrix}\begin{bmatrix}\Delta d_i(0)\\ \Delta v_i(0)\end{bmatrix} + \begin{bmatrix}-\frac{t^2}{2} - \tau^{*}t\\ -t\end{bmatrix} u_b \quad t \in [0, t_w]\\ \widetilde{\mathscr{M}}(t, t_w)\begin{bmatrix}\Delta d_i(t_w)\\ \Delta v_i(t_w)\end{bmatrix} \quad t \in (t_w, \infty)\end{cases} \tag{17}$$

Where, $\widetilde{\mathscr{M}}(t,t_0) = \begin{bmatrix} e^{z(t-t_0)}\cos y(t-t_0) - \frac{e^{z(t-t_0)}(\tau^{*}k_s - z)}{y}\sin y(t-t_0) & \frac{e^{z(t-t_0)}(1-\tau^{*}k_v)}{y}\sin y(t-t_0) \\ \frac{-k_s e^{z(t-t_0)}}{y}\sin y(t-t_0) & e^{z(t-t_0)}\cos y(t-t_0) - \frac{e^{z(t-t_0)}(k_v - z)}{y}\sin y(t-t_0)\end{bmatrix}$ represents a function of free response under an oscillatory ACC system.

Proposition 6. **(Overshoot condition)**: If **Proposition 2** holds, the overshoot is bound to happen. When the ACC system is impacted by bounded acceleration/deceleration, the first overshoot is in $t_{\Delta d,n}^{*}$, if Eq. (18-a) is satisfied. Alternatively, the first overshoot happens in $t_{\Delta d,l}^{*} = \frac{\pi + 2\arctan(B/A)}{2y} + t_w$, if either Eq. (18-b) or (18-c) is met. If Eq.(18-d) is satisfied, the first overshoot occurs at switch time t_w. Detailed proof has provided in **Appendix 4**.

$$\begin{cases} t_{\Delta d,n}^{*} \in [0, t_w] \\ \Delta d_i\left(t_{\Delta d,n}^{*}\right) * \Delta d_i(0) < 0 \end{cases} \tag{18-a}$$

$$\begin{cases} t_{\Delta d,n}^{*} \in [0, t_w] \\ \Delta d_i\left(t_{\Delta d,n}^{*}\right) * \Delta d_i(0) > 0 \\ \Delta d_i\left(t_{\Delta d,l}^{*}\right) * \Delta d_i(0) < 0 \end{cases} \tag{18-b}$$

$$\begin{cases} t_{\Delta d,n}^{*} \notin [0, t_w] \\ \Delta d_i(t_w) * \Delta d_i(0) > 0 \\ \Delta d_i\left(t_{\Delta d,l}^{*}\right) * \Delta d_i(t) < 0 \end{cases} \tag{18-c}$$

$$\begin{cases} t_{\Delta d,n}^{*} \notin [0, t_w] \\ \Delta d_i(t_w) * \Delta d_i(0) < 0 \end{cases} \tag{18-d}$$

Where, $A = (2z - \tau^{*}k_s)\Delta d_i(t_w) + (1 - \tau^{*}k_v)\Delta v_i(t_w)$ and $B = \left(-y - \frac{z(\tau^{*}k_s - z)}{y}\right)\Delta d_i(t_w) + \frac{z(1-\tau^{*}k_v)}{y}\Delta v_i(t_w)$.

Lemma 4. **(Overshoot condition)**: The first overshoot of ACC following linear control law ($t_w = 0$) happens in $t_{\Delta d,l}^{*} = \frac{\pi + 2\arctan(B/A)}{2y}$.

Proposition 7. **(Safety risk condition)**: The safety risk condition of **Scenario 1** under Proposition 2 is similar to **Proposition 5**, with the difference being the time of extremum clearance $t_{d,l}^{*}$ and its corresponding clearance $d_i\left(t_{d,l}^{*}\right)$. The proof is in **Appendix 5**.

From **Proposition 4** to **Proposition 7,** we can find that the safety and overshoot are jointly impacted by the vehicle's cut-in positions and speed, and the ACC design of the vehicle subject to cut-in maneuvers (manifested by λ_1 and λ_2) for Scenario 1. These four propositions significantly differ from stability analysis by Zhou et al., (2020), which is only related to the ACC control parameters. Moreover, the analytical derivation is extended to Scenario 2, which suggests that the safety and overshoot condition of the ACC system are further impacted by the deceleration and acceleration behavior of the cut-in vehicles.

3.3. Derivation of Scenario 2 under non-oscillatory ACC system

When the velocity of cut-in vehicles is not constant, as shown in Fig. 1, the analytical derivation is relatively complicated because of the existence of forced response. Note that the velocity profile under Scenario 2 is not differentiable, but the analysis remains feasible because the integral can be obtained in each piecewise interval. Moreover, ACC dynamic evolution exhibits continuity at the discontinuity points of given velocity profiles, as the states from the left and right intervals at these points are equivalent. To simplify the following analysis, the overshoot and safety analysis is conducted in each piece of given velocity profiles to ensure continuity. The nonlinear ACC interval and extremum of spacing response ($\Delta d_i(t)$), as well as extremum clearance ($d_i(t)$) in interval $[0, t_1]$, (t_1, t_2), and (t_2, ∞), is derived, respectively. By considering the result of all intervals, the nonlinear interval, overshoot, and safety condition of the entire cut-in process can be determined. Based on the velocity profile of Scenario 2, the nonlinear interval of ACC also starts from the initial, as long as the acceleration/deceleration of cut-in vehicle does not exceed the boundary. Yet, determining the switch time of nonlinear to linear control law is more complex due to the acceleration/deceleration change, as outlined in Proposition 3. Thus, we need to resort to Algorithm 1.

Algorithm 1. **(Switch time)**: According to the following steps, the ACC nonlinear interval $T_w = [0, t_w]$ could be obtained with similar logic of Eq. (7) in a segmented manner.

Input: $k_s, k_v, \tau^*, u_b, a_1, a_2, t_1, t_2, \Delta d_i(0), \Delta v_i(0)$ **Output:** t_w

revise Eq (7) to $A_1 t^2 + B_1 t + C_1 = 0$ (19-a) where $A_1 = \frac{k_s a_1 - k_s u_b}{2}, B_1 = k_s \Delta v_i(0) - k_s u_b \tau^* - k_v u_b + k_v a_1, C_1 = k_s \Delta d_i(0) + k_v \Delta v_i(0) - u_b$

solve Eq. (19-a)

if: roots of Eq. (19-a) are not real numbers or $t_{s,1} = \max(\text{roots of Eq. (19-a)}) < 0$:

  ACC follows linear feedback control law in all intervals

else:

  if: $t_{s,1} \le t_1$

    $t_w = t_{s,1}$

  else:

    calculate $\Delta d_i(t_1), \Delta v_i(t_1)$ based on bounded acceleration/deceleration law

    revise Eq (7) to $A_2 t^2 + B_2 t + C_2 = 0$ (19-b) where $A_2 = \frac{k_s a_2 - k_s u_b}{2}, B_2 = k_s \Delta v_i(t_1) - k_s u_b \tau^* - k_v u_b + k_v a_2, C_2 = k_s \Delta d_i(t_1) + k_v \Delta v_i(t_1) - u_b$

    solve Eq. (19-b) and obtain $t_{s,2} = \max(\text{roots of Eq. (19-b)})$

    if: $0 < t_{s,2} < t_2 - t_1$

      $t_w = t_1 + t_{s,2}$

    else:

      calculate $\Delta d_i(t_2), \Delta v_i(t_2)$ based on bounded acceleration/deceleration law

      revise Eq (7) to $A_3 t^2 + B_3 t + C_3 = 0$ (19-c) where $A_3 = -\frac{k_s u_b}{2}, B_3 = k_s \Delta v_i(t_2) - k_s u_b \tau^* - k_v u_b, C = k_s \Delta d_i(t_2) + k_v \Delta v_i(t_2) - u_b$

      solve Eq. (19-c) and obtain $t_{s,3} = \max(\text{roots of Eq. (19-c)})$

      $t_w = t_2 + t_{s,3}$

The switch time of linear and nonlinear control law is impacted by the forced response, so we consider the most representative case $t_w < t_1$ to conduct the following derivation ACC dynamic evolution. In this condition, the ACC dynamic evolution under Scenario 2 can be represented as:

$$\begin{bmatrix} \Delta d_i(t) \\ \Delta v_i(t) \end{bmatrix} = \begin{cases} \begin{bmatrix} 1 & t \\ 0 & 1 \end{bmatrix} \begin{bmatrix} \Delta d_i(0) \\ \Delta v_i(0) \end{bmatrix} + \begin{bmatrix} -\frac{t^2}{2} - \tau^* t \\ -t \end{bmatrix} u_b + a_1 \begin{bmatrix} \frac{t^2}{2} \\ t \end{bmatrix} t \in [0, t_w] \\ M(t, t_w) \begin{bmatrix} \Delta d_i(t_w) \\ \Delta v_i(t_w) \end{bmatrix} + a_1 F(t, t_w) t \in (t_w, t_1] \\ M(t, t_1) \begin{bmatrix} \Delta d_i(t_1) \\ \Delta v_i(t_1) \end{bmatrix} + a_2 F(t, t_1) t \in (t_1, t_2] \\ M(t, t_2) \begin{bmatrix} \Delta d_i(t_2) \\ \Delta v_i(t_2) \end{bmatrix} t \in (t_2, \infty) \end{cases} \tag{20}$$

Where $\mathscr{F}(t, t_0) = \begin{bmatrix} \frac{(1 - \tau^* k_{vi})}{\lambda_1 - \lambda_2} \left(\frac{1}{\lambda_1} e^{\lambda_1 (t - t_0)} - \frac{1}{\lambda_2} e^{\lambda_2 (t - t_0)} + \frac{1}{\lambda_2} - \frac{1}{\lambda_1} \right) \\ \frac{(-\lambda_2 - k_{vi})}{\lambda_1 - \lambda_2} \left(\frac{1}{-\lambda_1} + \frac{1}{\lambda_1} e^{\lambda_1 (t - t_0)} \right) + \frac{(\lambda_1 + k_{vi})}{\lambda_1 - \lambda_2} \left(\frac{1}{-\lambda_2} + \frac{1}{\lambda_2} e^{\lambda_2 (t - t_0)} \right) \end{bmatrix}$ represents the function of forced response under non-oscillatory ACC system mapping $x_i(t_0)$ and $x_i(t)$.

Lemma 5. **(Overshoot condition)**: Derivation of overshoot condition under Scenario 2 is similar to **Proposition 4**, whereas the

overshoot condition needs to examine interval by interval. We take $t \in (t_w, t_1]$ to illustrate the process. When $t \in (t_w, t_1]$, ACC dynamic evolution is in Eq. (21-a), and the time of extreme spacing response could be obtained in Eq. (21-b). if either of $0 < t_o^* < t_1$ and $\Delta d_i(t_o^*) \bullet \Delta d_i(0) < 0$, or $\Delta d_i(t_1) \bullet \Delta d_i(0) < 0$ is satisfied, the overshoot will occur in $(t_w, t_1]$. Otherwise, the overshoot does not exist in $(t_w, t_1]$. When there is no overshoot in all intervals, then the ACC system has no overshoot in the entire cut-in process. If t_o^* does not exist, it indicates the ACC dynamic evolution is smooth, but it may not be safe because the initial cut-in condition may be risky, as shown in **Fig 2**.

$$\Delta d_i(t) = e^{\lambda_1(t-t_w)}\Delta d_i(t_w) - \frac{e^{\lambda_1(t-t_w)} - e^{\lambda_2(t-t_w)}}{\lambda_1 - \lambda_2}(\lambda_1 + \tau^* k_s)\Delta d_i(t_w) + \frac{e^{\lambda_1(t-t_w)} - e^{\lambda_2(t-t_w)}}{\lambda_1 - \lambda_2}(1 - \tau^* k_v)\Delta v_i(t_w)$$

$$+ \frac{a_1(1 - \tau^* k_{vi})}{\lambda_1 - \lambda_2}\left(\frac{1}{\lambda_1}e^{\lambda_1(t-t_w)} - \frac{1}{\lambda_2}e^{\lambda_2(t-t_w)} + \frac{1}{\lambda_2} - \frac{1}{\lambda_1}\right) \tag{21-a}$$

$$t_o^* = \frac{\ln\frac{-N}{M}}{\lambda_1 - \lambda_2} + t_w \textit{(21-b)}$$

Where $N = \frac{(\lambda_1 + \tau^* k_s)\Delta d_i(t_w) - (1 - \tau^* k_v)\Delta v_i(t_w)}{\lambda_1 - \lambda_2} - \frac{a_1(1 - \tau^* k_{vi})}{\lambda_1 - \lambda_2}\frac{1}{\lambda_2}$ and $M = \lambda_1 \Delta d_i(t_w) + \frac{(1 - \tau^* k_v)\Delta v_i(t_w) - (\lambda_1 + \tau^* k_s)\Delta d_i(t_w)}{\lambda_1 - \lambda_2} + \frac{a_1(1 - \tau^* k_{vi})}{\lambda_1 - \lambda_2}\frac{1}{\lambda_1}$

Lemma 6. **(Safety risk condition)**: Derivation of safety condition is also conducted under each piece interval. We take $t \in [0, t_w]$ as an example. Based on Eq. (16-a), the distance gap evolution is shown in Eq. (22-a). If either of $t_s^* \in [0, t_w]$ and $\min(d_i(0), d_i(t_s^*)) \le \varepsilon$, or $t_s^* \notin [0, t_w]$ and $\min(d_i(0), d_i(t_w)) \le \varepsilon$ is satisfied, the vehicle subjected to cut-in maneuvers have safety risk.

$$d_i(t) = \frac{(a_1 - u_b)t^2}{2} + \Delta v_i(0)t + \Delta d_i(0) + v_i(0)\,\tau^* \tag{22-a}$$

$$t_s^* = \frac{\Delta v_i(0)}{u_b - a_1} \tag{22-b}$$

The detailed ACC dynamic evolution of oscillatory system under Scenario 2 is provided in **Appendix 6**. While the derivations based on these two scenarios are representative (Li et al., 2021; Sharma et al., 2019), the actual cut-in trajectory is more complex than these two scenarios, especially under the traffic oscillation. As discussed in Li et al. (2014), each trajectory could be treated as a superposition of a stationary component (i.e., average speed and spacing) and an oscillation component (i.e., sinusoidal fluctuation). In Scenario 1, the ACC dynamic evolution under stationary component has been derived. Consequently, **Appendix 7** presents the dynamic evolution of non-oscillatory ACC system under oscillatory cut-in speed (i.e., $a_{i-1}(t) = M\sin wt$), as an example to demonstrate the genericity of the proposed framework.

4. Analysis of Numerical Experiment

In this section, we perform numerical experiments to have a comprehensive understanding of the overshoot and safety conditions under Scenario 1 and 2, respectively. Specifically, the numerical experiment considers particular numeric cases, and it differentiates from numerical simulation as solutions are derived analytically. The numerical experiment can be divided into three parts: (i) case studies; (ii) sensitivity analysis of control parameters; (iii) commercial ACC evaluations using calibrated control parameters (Jiang et al., 2023; Y. Zhou et al., 2022). The default parameter settings for experiments are given in Table 1.

Considering Table 1, Proposition 1 and 2, we can find the region where the eigenvalue of A_d is real/complex, and the region of string stability (Chen et al., 2021) in Fig. 3**(a-c)** under different constant time gap. Note that the real eigenvalue of A_d indicates the non-oscillatory ACC system, whereases a complex eigenvalue signifies an oscillatory system. In Fig. 3, it is explicitly shown that the string stability and non-oscillation of ACC itself are two distinct properties. The boundary between non-oscillatory and oscillatory ACC systems is nonlinear with respect to control parameters, but the boundary between string stability and string instability is linearly separated. With the increase of the constant time gap, the string stability of the ACC system is enhanced accordingly. Meanwhile, the region of the oscillatory ACC system decreases, aligning with **Propositions 1 and 2**. Specifically, maintaining a larger constant time gap promotes a more non-oscillatory ACC system. The lower bound of k_s and k_v to ensure a non-oscillatory system both decrease as τ^* enlargers, although k_s is more sensitive compared to k_v. Given an identical constant time gap, as k_s increase, the oscillatory region

Table 1
Default value setting for numerical experiments.

Parameters	Value	Parameters	Value
τ^*	1.0 sec	$\Delta d_{i-1}(t_0)$	(-20 *m*, 10 *m*)
k_s	1.2	k_v	1.0
δ_i^*	5 *m*	$\Delta v_{i-1}(t_0)$	(-20 *m/s*, 10 *m/s*)
$v_{initial}$	20 *m/s*	t_0	0 *s*
a_1	-2 *m/s*^{2}	t_1, t_2	4 *s*, 8 *s*
a_2	2 *m/s*^{2}	Threshold of safety risk (ε)	2 *m*

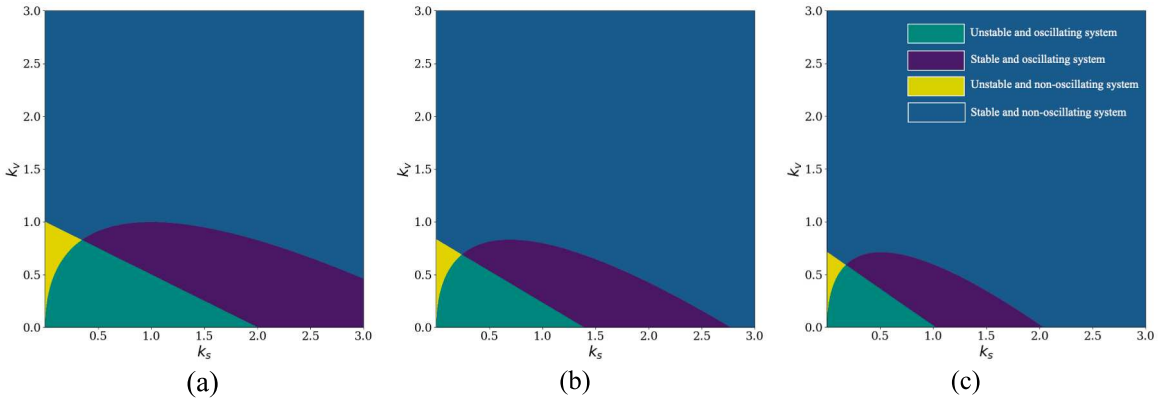

Fig. 3. System string stability and oscillation region for different feedback gains.

initially expands before contracting. However, with an increase in k_v, the region of the oscillatory system consistently shrinks. However, it is important to acknowledge that although larger control parameters (i.e., constant time gap, spacing and velocity gain) enhance the non-oscillation and string stability domain of the ACC system, there is still a possibility of encountering overshoot and potential safety concerns under string-stable and non-oscillatory ACC system, arising from external disturbance (i.e., initial cut-in condition and following driving behavior). Therefore, the following case study presents the ACC dynamic evolution under various specific cut-in maneuvers to investigate the impact of cut-in behaviors on overshoot and safety risk conditions.

4.1. Cases analysis of cut-in maneuvers

In this section, we select $k_s = 1.2$, $k_v = 1.0$ and $\tau^* = 1$ to make the ACC system non-oscillatory and string-stable for illustration purposes. To better highlight the impacts rendered by cut-in maneuvers (i.e., initial cut-in condition and velocity change of the cut-in vehicle), Ten cut-in conditions are designed as Table 2. We adjust the initial spacing deviation and velocity deviation respectively between vehicle i and cut-in vehicle $i-1$ under negative and positive initial deviations from the equilibrium. The negative/positive initial spacing deviation indicates the cut-in maneuver is aggressive/conservative (i.e., initial cut-in spacing is less/more than equilibrium spacing). On the other hand, the negative/positive initial velocity deviation represents that the cut-in velocity is slower/faster than that of the subjected vehicle. We design two sets of cases to analyze the impact of cut-in maneuvers on overshoot and safety risk conditions. In the cases of overshoot, we focus more on the positive initial spacing deviation, because it is more likely to lead to overshoot. In safety-critical cases, we are more concerned with aggressive cut-in maneuvers with different initial velocity deviations.

Fig. 4 illustrates spacing trajectories and deviations from equilibrium spacing in two scenarios. In Scenario 1, the initial velocity deviation can disrupt the initial spacing equilibrium (case 1), but the temporary spacing deviation is not overshoot because the response remains consistently positive without change in sign. A similar phenomenon is also shown in case 3 when the initial spacing is not in equilibrium. When velocity equilibrium is initially maintained (case 2), spacing eventually returns to equilibrium without overshoot. For combined spacing and velocity deviation (cases 4, 5), larger initial cut-in spacing prevents overshoot for slow cut-in velocity (case 4), but excessively slow cut-in velocity can lead to negative overshoot (case 5). Therefore, differences in signs of initial spacing and velocity deviation tend to cause overshoot. Fig. 4**(a-2)** illustrates the safety-critical cases, characterized by aggressive cut-in maneuvers. If the initial spacing is adequate, a relatively slow cut-in speed may not lead to a collision or potential collision (case 6). A comparatively faster cut-in speed can mitigate the effects of a negative initial spacing deviation (case 9). When cut-in spacing is less than equilibrium but cut-in velocity matches equilibrium (case 7), the situation is also safe, as subsequent spacing is gradually increased. The highest risk, however, arises when both spacing and velocity deviations are negative (cases 8, 10). Under these conditions, as the cut-in velocity decreases, the safety risk condition transitions from potential collision to collision.

In Scenario 2, the velocity dip of cut-in vehicle introduces more cut-in disturbances. Initial deceleration reduces positive velocity deviations in overshoot cases, further reducing spacing deviations (cases 1, 3). However, if initial velocity deviation is negative, deceleration worsens ACC dynamics due to forced response, intensifying negative overshoot (cases 4, 5). Minor impacts of velocity dip on spacing response are seen when initial velocity deviation is in equilibrium (case 2). Fig 4**(b-2)** shows increased safety risks during

Table 2
Case design setting for initial cut-in condition.

Overshoot Cases	$\Delta d_i(t_0)$[m]	$\Delta v_i(t_0)$[m/s]	Safety-critical Cases	$\Delta d_i(t_0)$[m]	$\Delta v_i(t_0)$[m/s]
#1	0	8	#6	0	−8
#2	10	0	#7	−10	0
#3	10	8	#8	−10	−8
#4	10	−8	#9	−10	8
#5	10	−12	#10	−10	−12

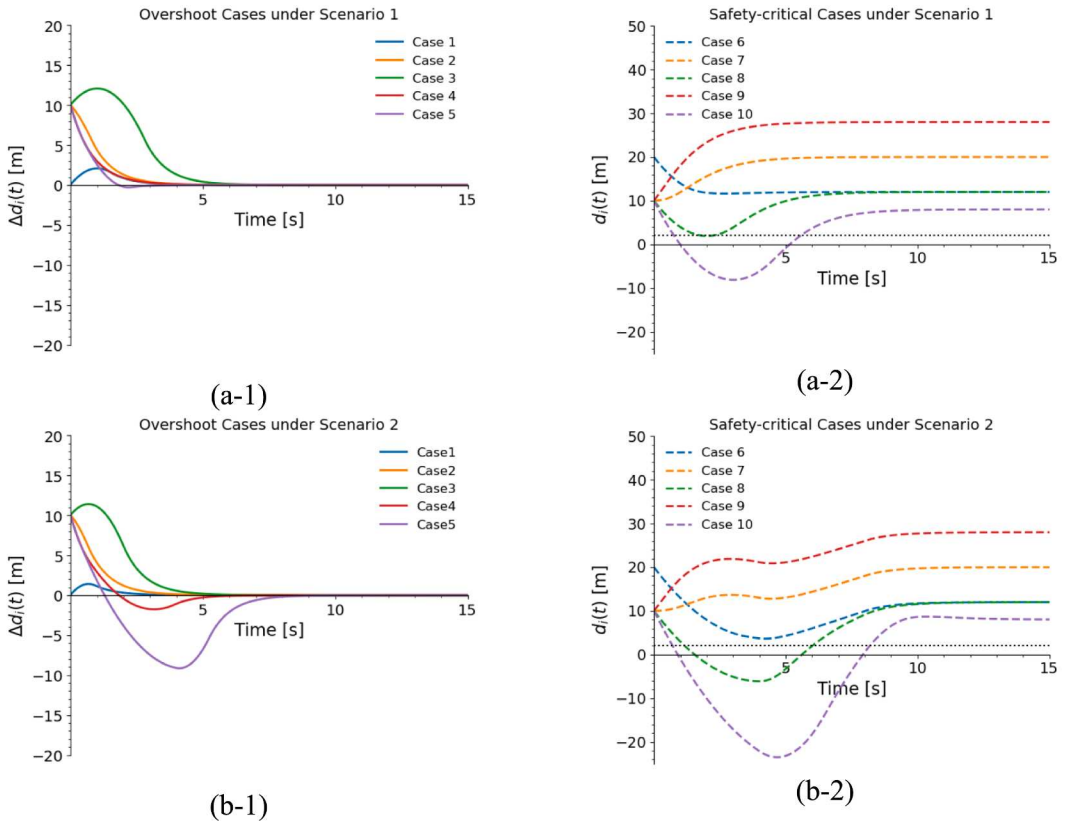

Fig. 4. Overshoot and safety–critical cases analysis under different cut-in conditions in Scenario 1 and Scenario 2 (Black dotted line in (a-2) and (b-2) indicates the threshold of safety risk).

the deceleration period (0s to 4s), particularly for negative initial velocity deviation cases (6,8,10). This highlights cut-in vehicle behavior's link to overshoot and safety conditions of ACC dynamic.

4.2. Sensitivity analysis for control parameters

For a more comprehensive understanding of the ACC system under cut-in maneuvers, we set the range of the initial spacing deviation and velocity deviation $\Delta d_{i-1}(t_0) \in [-20m, 10m]$, $\Delta v_{i-1}(t_0) \in [-20m/s, 10m/s]$, with 0.125 m (or m/s) as a resolution, to conduct a series of sensitivity analysis for control parameters. To quantify the result, we employ event frequency (i.e., safety risk and positive/negative overshoot) across all initial cut-in conditions (57,600 = 30/0.125 × 30/0.125) as a metric. Note that both collision and potential collision are considered as safety risks. A larger metric suggests the event occurs more frequently.

The event frequencies under different control parameters are detailed in Table 3. The results of Scenario 1, as presented in Fig. 5**(a-1) to 5(a-3)**, show that when the spacing feedback gain increase, the safety of ACC is slightly compromised (safety risk frequency from 38.52% to 38.63%). It is because the larger feedback gain more readily triggers the bounded acceleration and deceleration (refer to Eq. (11)), resulting in a longer response time. Therefore, handling safety-critical conditions becomes challenging. According to Eq. (17),

Table 3
Event frequency under different parameters setting in Scenario 1.

Parameters	Safe but with positive overshoot (%)	Safety but with negative overshoot (%)	Potential collision (%)	Rear-end collision (%)
a-1	1.04	4.17	5.62	32.90
a-2 (k_s ↑)	1.80 ↑	4.54 ↑	5.63 ↑	32.92 ↑
a-3	2.93 ↑	4.84 ↑	5.64 ↑	32.99 ↑
b-1	1.15	4.06	5.62	32.90
b-2 (k_v ↑)	1.40 ↑	4.30 ↑	5.62 →	32.90 →
b-3	1.56 ↑	4.46 ↑	5.62 →	32.90 →
c-1	1.00	4.71	2.54	27.27
c-2 (τ^* ↑)	1.88 ↑	6.07 ↑	2.17 ↓	22.77 ↓
c-3	3.27 ↑	7.61 ↑	1.95 ↓	18.77 ↓

Notes: the symbol denotes the increase (↑), decrease (↓), and unchanged (→) correlating with an increase in control parameters.

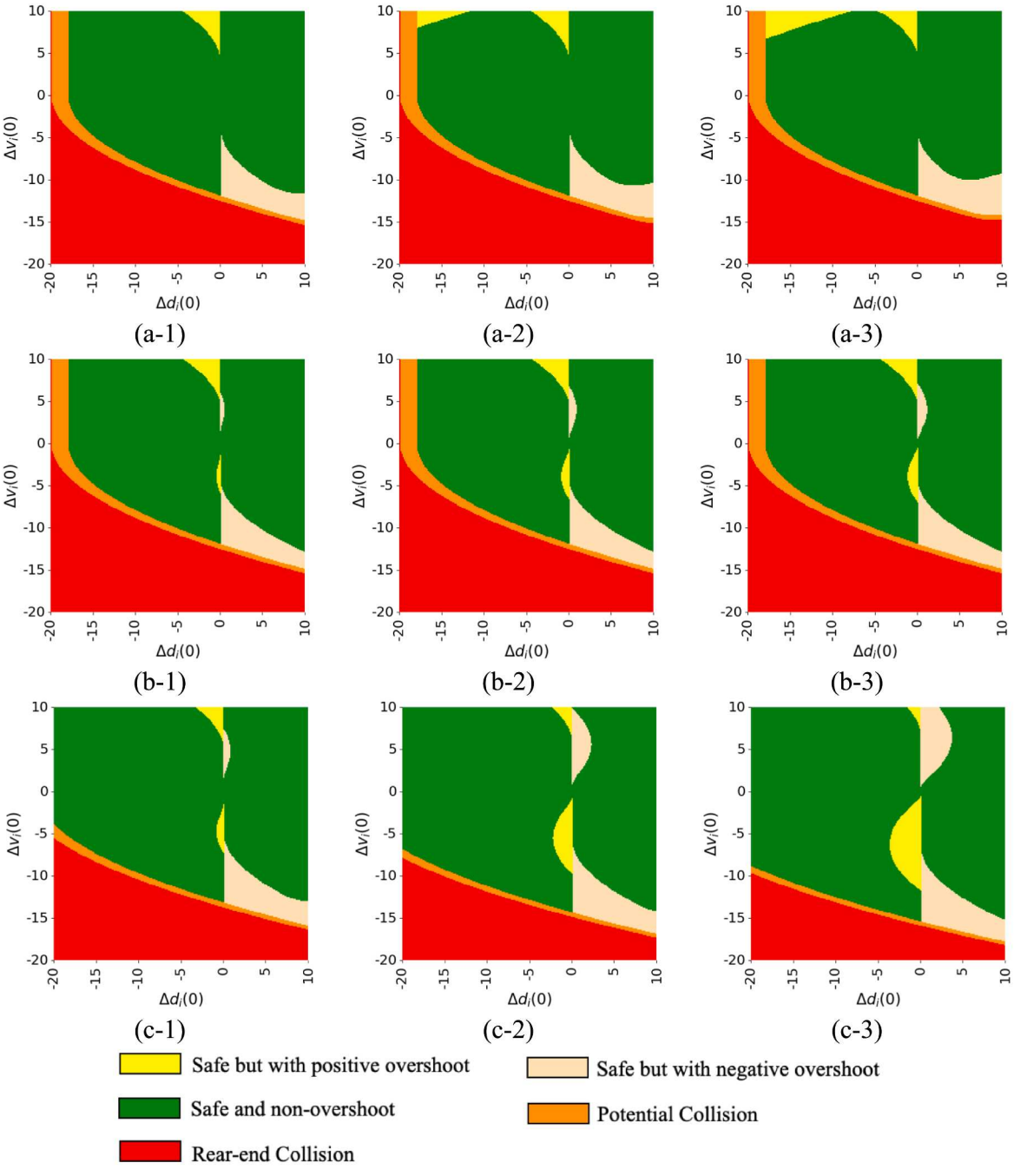

Fig. 5. Sensitivity analysis for feedback gain and initial cut-in condition under Scenario 1: (a) spacing gain; (b) velocity gain; (c) constant time gap.

term $\frac{e^{\lambda_1(t-tw)}-e^{\lambda_2(t-tw)}}{\lambda_1-\lambda_2}$ is consistently non-negative due to $\lambda_1 > \lambda_2$, and term $\lambda_1 + \tau^* k_s$ increase with an increase in k_s. Consequently, $\Delta d_i(t)$ is more likely to have a different sign with $\Delta d_i(0)$, which leads to overshoot appearing more often (negative overshoot from 4.17% to 4.84%; positive overshoot from 1.04% to 2.93%). Increasing velocity gain has a similar pattern from the perspective of overshoot (negative overshoot from 4.06% to 4.46%; positive overshoot from 1.15% to 1.56%), as shown in Fig. 5**(b-1)** to **5(b-3)**. Comparatively, k_s exert larger impacts than k_v. One plausible explanation is that spacing disturbance is the predominant disturbance under Scenario 1, and a larger k_s could potentially lead to an overreaction of the ACC system to such disturbance.

From Fig. 5**(c-1)** to **5(c-3)**, the larger constant time gap could enhance the safety (safety risk from 29.81% to 20.72%) but increase the occurrence of overshoot (positive overshoot from 1.00% to 3.27%; negative overshoot from 4.71% to 7.61%). The reason is that,

when the constant time gap increases, the magnitude of eigenvalues of A_d also increases, which results in a more aggressive response for the ACC system to equilibrium and hence triggers an overshoot by Proposition 1 and Eq. (14). As τ^* gradually increases, there is a corresponding decrease in the margin gain for safety. Conversely, the regime where overshoot occurs experiences a significant expansion.

Under Scenario 2, the velocity dip of the cut-in vehicle will elevate impacts on safety and overshoot significantly, as in Fig. 6. When the cut-in vehicle decelerates initially, it could render a greater likelihood of safety risk than Scenario 1 (safety risk probability under default setting (a-1) from 38.52% to 47.87%), as shown in Table 4. Besides, increasing the spacing gain could subtly broaden the region of negative overshoot and unsafe conditions, particularly when the initial cut-in spacing is larger ($5m \leq \Delta d_i(0) \leq 10m$), and the

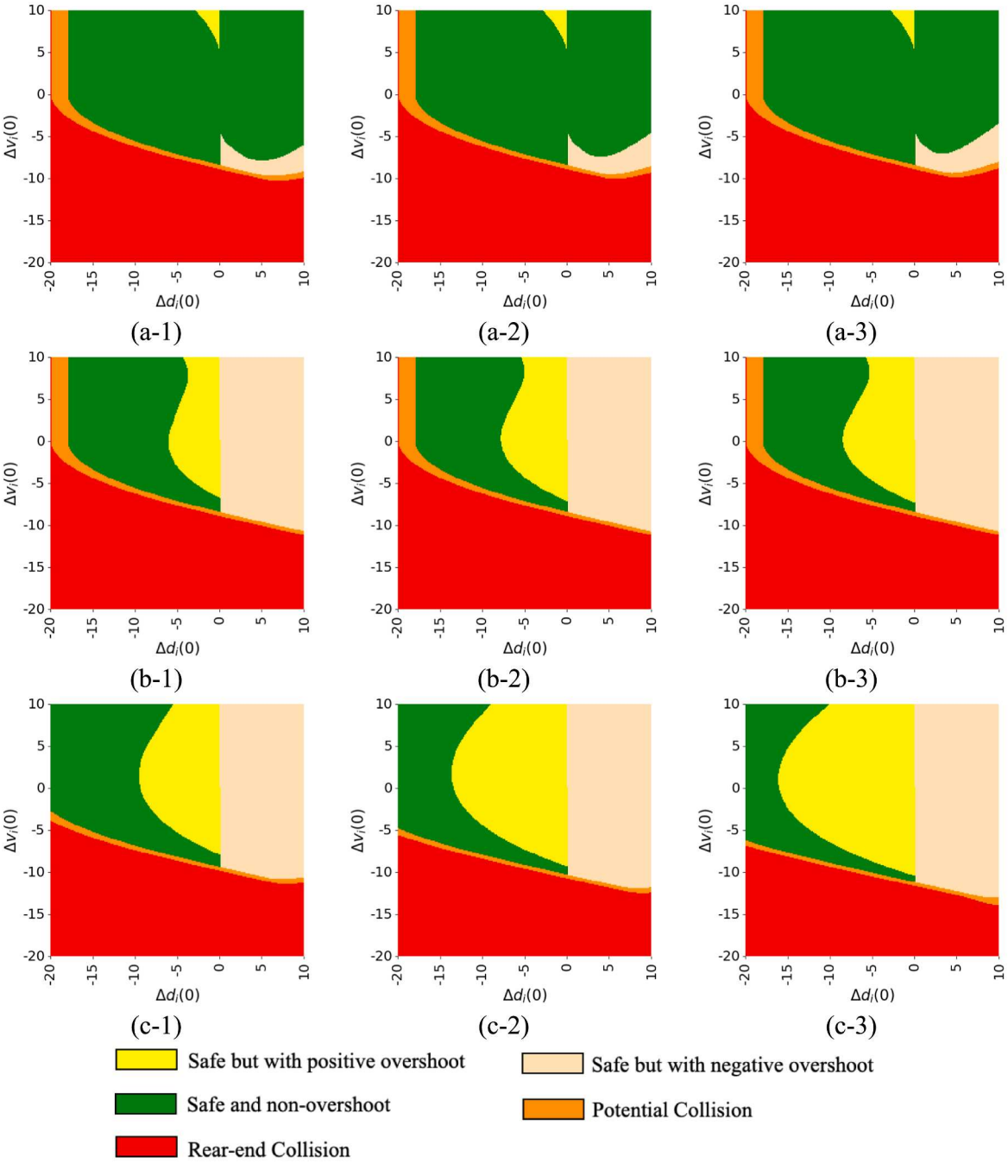

Fig. 6. Sensitivity analysis for feedback gain and initial cut-in condition in Scenario 2: (a) spacing gain; (b) velocity gain; (c) constant time gap.

Table 4
Event frequency under different parameters setting in Scenario 2.

Parameters	Safe but with positive overshoot (%)	Safety but with negative overshoot (%)	Potential collision (%)	Rear-end collision (%)
a-1	0.63	2.46	4.81	43.06
a-2 (k_s ↑)	0.63 →	2.95 ↑	4.82 ↑	43.27 ↑
a-3	0.63 →	3.37 ↑	4.85 ↑	43.48 ↑
b-1	8.42	22.05	4.70	42.79
b-2 (k_v ↑)	11.24 ↑	22.05 →	4.70 →	42.79 →
b-3	12.18 ↑	22.05 →	4.70 →	42.79 →
c-1	14.54	22.86	1.97	38.73
c-2 (τ^* ↑)	22.81 ↑	23.95 ↑	1.73 ↓	35.21 ↓
c-3	28.40 ↑	24.99 ↑	1.70 ↓	31.89 ↓

longitudinal velocity of the cut-in vehicle is slower than the subjected vehicle ($-10m/s \leq \Delta v_i(0) \leq -5m/s$). The negative overshoot caused by the large initial velocity deviation in Scenario 1, as depicted in Fig. 5**(a-3)**, is mitigated by the cut-in vehicle's velocity drop. Moreover, the escalation of the velocity gain, demonstrated in Fig. 6**(b-1)** to **6(b-3)**, amplifies the velocity perturbations under Scenario 2. This may be because the ACC system behaves more aggressively to attain the velocity of cut-in vehicle, but its velocity is fluctuated, which results in a more extensive region of overshoot than Scenario 1 (overall overshoot in (b-1) from 5.21% to 30.47%). The pattern of τ^* aligns with that of Scenario 1, but the velocity drop by the cut-in vehicle exacerbates the overshoot conditions, notably negative overshoot. A dramatic increase in overshoot frequency is observed from Fig. 6**(a) to 6(b)**. This is because when $k_v = 1.0$ and τ^*=1.0, λ_1 is consistently equal to -1 and unaffected by changes in k_s (refer to Eq. (7)). Conversely, λ_2 decreases as k_s increases. In control parameters setting in Fig. 6**b**, λ_1 increase and λ_2 decrease with the increase of k_v. It will cause a more rapid response (refer to Eq. (14)) and the overshoot condition is correspondingly escalated due to the impact of velocity dip in Scenario 2.

Based on the outcomes of the two scenarios, there are three main insights: (i) k_s and k_v have a minor impact on safety under cut-in maneuver; (ii) increases in spacing or velocity gains may intensify the corresponding disturbance and further exacerbate the overshoot, especially when the increased control gain is consistent with the predominate disturbance (e.g., Fig 5**(a) and 6(b)**); (iii) τ^* is strongly related to the safety condition, but it exhibits a trade-off with the frequency of overshoot occurrences.

4.3. Analysis of commercial ACC

In this section, we apply the proposed framework to analyze the performance of commercial ACC systems subject to cut-in ma-

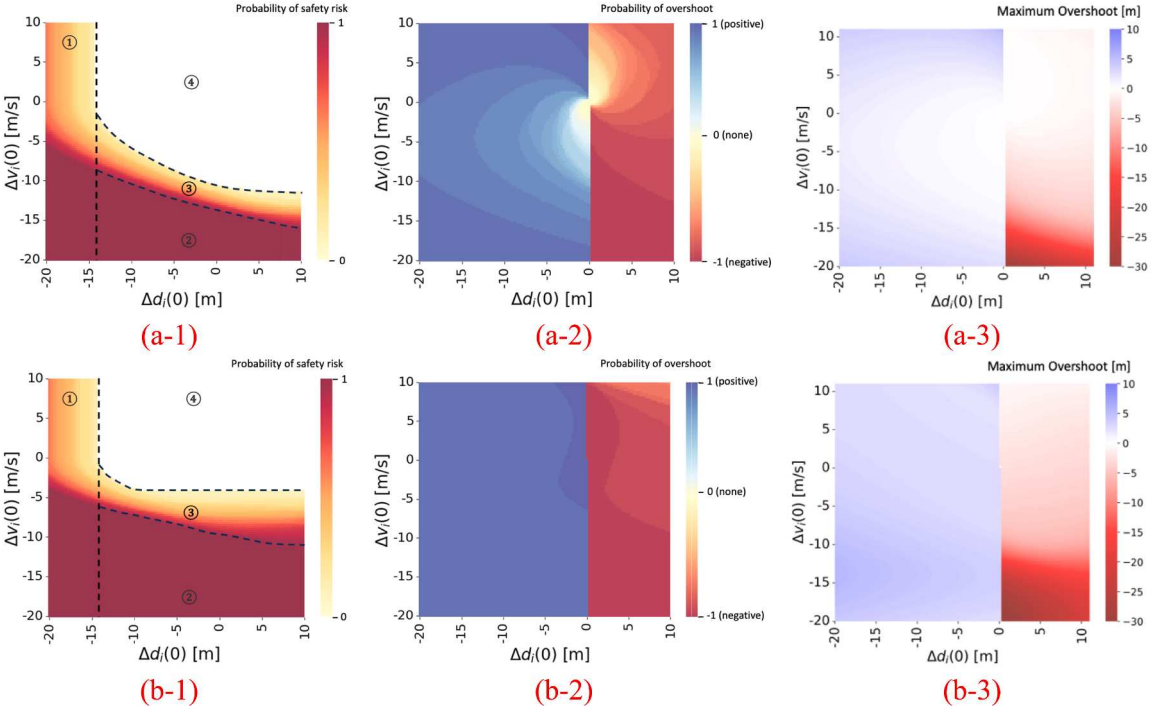

Fig. 7. Probabilistic safety risk and overshoot condition under Scenario 1 (a) and Scenario 2 (b): (1) probability of safety risk, (2) probability of overshoot, (3) expected maximum overshoot.

neuvers to have a practical understanding of ACC safety and overshoot boundaries. The field test ACC data is from (Li et al., 2022), in which the designed speed profile is similar to Scenario 2. Based on that, the empirical joint distributions of control parameters for the second-order linear ACC system are calibrated by approximated Bayesian computation approach (Jiang et al., 2023; Zhou et al., 2022b). In this section, we randomly sample 50 parameters set from the calibrated joint distributions of k_s, k_v, δ_i^*, τ^*, l_i to examine the probability of the overshoot and safety conditions, based on the derivations given in Section 3. Specifically, each control parameter set can identify whether safety risk and overshoot happen (as exemplified in Figs. 5 and 6). By aggregation, we can collectively obtain the probability for those two conditions. In the safety analysis (Fig. 7**(a-1)** and **(b-1)**), when the cut-in maneuvers are extremely aggressive, with cut-in spacing substantially smaller than equilibrium (area 1), the larger cut-in longitudinal velocity could avoid collision, but still have near-collision risk. However, when the cut-in longitudinal velocity is much smaller than the following ACC vehicle (area 2), increasing the cut-in spacing is not able to avoid a collision. By comparing area 3 under scenarios 1 and 2, the temporary velocity drop of the cut-in vehicle can further increase the rear-end collision risk, resulting in the lower and upper boundary of area 3 increase. These changes signify that temporary velocity drops decrease the tolerance of ACC for extreme initial spacing and velocity deviations. From area 4, we can find that the positive velocity deviation ($\Delta v_i(0) \geq 0$) with reasonable cut-in spacing ($\Delta d_i(0) \geq -10$) is the critical indicator for the safety of the ACC system under cut-in maneuvers in both scenarios. In overshoot analysis, under Scenario 1, the probability of overshoot is centered on the equilibrium and increases in a spiral outward. When initial spacing deviation is near equilibrium but with excessive velocity deviation, overshoot is most likely to occur (e.g., $\Delta d_i(0) = -1$ and $\Delta v_i(0) = 10$; $\Delta d_i(0) = 5$ and $\Delta v_i(0) = -15$). Under Scenario 2, the velocity dip of the cut-in vehicle amplifies overshoot likelihood. However, larger initial conditions, as in Fig. 7**(b-2)**, can mitigate overshoot. For instance, negative overshoot probability decreases from 100% to 86% when initial deviations (i.e., $\Delta d_i(0)$ and $\Delta v_i(0)$) both transition from 1 to 10. For each set of control parameters and given cut-in maneuver, the maximum overshoot can be derived. The expected value of maximum overshoot for a given cut-in maneuver is then visualized by averaging maximum overshoot across the selected joint distributions of control parameters, as shown in Figs. 7**(a-3)** and **7(b-3)**. It is observed that when cut-in vehicles experience a velocity dip, there is an increase in both the magnitude of overshoot and the likelihood of an overshoot condition.

Section 4.2 underscores that by adjusting the control parameters, we can significantly mitigate the safety risks and overshoot situations that occur with the ACC system during cut-in maneuvers. However, the analysis of commercial ACC systems suggests a safety inadequacy with SAE Level 2 AV (Knoop et al., 2019), particularly in scenarios involving slower cut-in vehicles and aggressive cut-ins. In order to address this concern, it is crucial that Level 2 AVs are equipped with advanced anticipatory abilities for cut-in maneuvers, for example, a more refined perception and communication system (van Arem et al., 2006) and more accurate trajectory prediction models (Chen et al., 2023; Wang et al., 2015). Based on these anticipatory measures, the ACC system could then proactively determine optimal driving behavior to maintain both traffic safety and efficiency. For instance, when the initial cut-in condition falls into areas 1 and 2, the system could prioritize overtaking the cut-in vehicle to avoid a collision. Conversely, if the cut-in condition falls into area 3, the subjected vehicle could slow down and yield to the cut-in vehicle, enabling a safe and non-overshoot ACC dynamic subject to cut-in maneuvers. These proactive and predictive strategies offer promising pathways to significantly enhance the safety performance of Level 2 AV. More importantly, the proposed framework provides not only instructive insights on ACC design, but a more comprehensive assessment of safety risk and overshoot conditions based on cut-in trajectory. If we incorporate the safety and overshoot evaluation results into the control logic, this feature will significantly improve the ACC system's ability to determine the most suitable driving behavior in response to cut-in disturbances. When the cut-in maneuver is given, a feasible region of control gain for a linear ACC system can be identified to ensure safety and manage overshoot. As depicted in Fig. 8, the control gains within the intersection of the green region in Fig. 8**(a)** and the white region in Fig. 8**(b)** should be selected for the linear ACC system to maintain safety and prevent overshoot under the given cut-in disturbance. The proposed framework enables the linear feedback control to adaptively adjust the control gains, addressing the limitations of linear feedback controllers in guaranteeing safety constraints over cut-in scenarios. In other words, with the help of the proposed framework, the linear ACC can achieve maximum effectiveness in ensuring safety and stability.

5. Conclusion

This study proposes a theoretical and analytical framework to model the ACC dynamic evolution in response to cut-in disturbances, embedded with bounded acceleration/deceleration, a primary nonlinear characteristic of the ACC system. We first apply the Caley-Hamilton theorem to derive the general ACC dynamic evolution based on second-order linear feedback control. Through the derivation, we show that while control parameters govern the ACC system's inherent oscillation nature, the initial condition and subsequent behavior of the cut-in vehicle will collectively influence the system's safety and overshoot. We also define safety risk as the distance gap between the subjected vehicle and the cut-in vehicle is smaller than a pre-defined threshold. Two representative cut-in velocity profiles (i.e., constant velocity and a velocity dip) are considered, and sufficient and necessary conditions for ensuring safety and non-overshoot, regardless of local and string stability, are derived. Notably, the proposed framework systematically incorporates control parameters, initial cut-in conditions, and cut-in behavior, thereby addressing the limitations of local/string stability analysis from a safety perspective.

A series of numerical experiments have been conducted to gain a comprehensive and fine-grained understanding. Specifically, the case analysis of several initial cut-in conditions has validated that the cut-in maneuver is significantly related to the safety and stability of the ACC system, and excessive negative overshoot may lead to rear-end collision risk. Then, we examine the impact of control parameters on safety and overshoot by sensitivity analysis under various initial cut-in conditions. The results unveil that (i) cut-in with

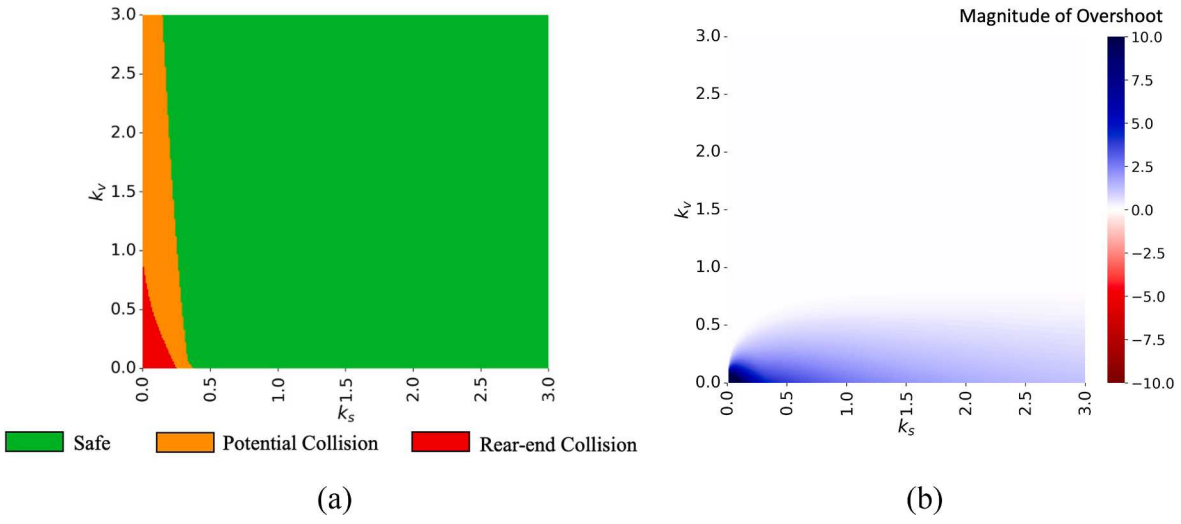

Fig. 8. Feasible region of control gain for linear ACC to ensure safety and non-overshoot under given cut-in maneuver ($\Delta d_i(0) = -10m$ and $\Delta v_i(0) = -8m/s$ under Scenario 1).

a dip profile has a severe impact on exacerbating the safety risk and instability; (ii) increasing spacing and velocity gain may exacerbate cut-in disturbance but have a minor impact on safety; (iii) while adopting a larger constant time gap can enhance safety, it's also important to consider its potential to increase the occurrence of overshoot conditions. Moreover, by adopting the field-tested parameters, we have provided the probabilistic safety and non-overshoot region for commercial ACC systems under different cut-in maneuvers. Finally, this paper sheds light on the understanding ACC system under cut-in scenarios and further provides physical insight to design a more robust, safe, and stable ACC system.

While the proposed framework offers instructive insights, it could be further enhanced in several ways for future research. The framework incorporates the nonlinear factor (i.e., acceleration/deceleration boundary) of the linear ACC system, further consideration of factors such as control actuation delay, sensing delay, and nonlinear vehicle dynamics (Orosz, 2016; Treiber et al., 2006; Zhang et al., 2018) could lead to a more comprehensive understanding of the ACC systems. For nonlinear systems, as well as delayed systems, numerical approximations (e.g., Runge-Kutta methods and Padé approximation) are usually needed. This is because providing an analytical framework for nonlinear systems is very challenging due to the limitations of mathematical tools. Furthermore, future research could explore a broader range of cut-in scenarios to enrich the case analysis. However, it is important to note that the proposed framework remains applicable and valid in these additional contexts.

CRediT authorship contribution statement

Zihao Li: Conceptualization, Formal analysis, Methodology, Validation, Visualization, Writing – original draft. **Yang Zhou:** Conceptualization, Formal analysis, Funding acquisition, Methodology, Supervision, Writing – review & editing. **Danjue Chen:** Conceptualization, Formal analysis, Writing – review & editing. **Yunlong Zhang:** Conceptualization, Supervision, Writing – review & editing.

Declaration of competing interest

The authors declare that they have no known competing financial interests or personal relationships that could have appeared to influence the work reported in this paper.

Acknowledgment

We would like to thank the anonymous reviewers for all their valuable comments and suggestions, which helped us to improve the quality of the manuscript. This research is supported by the Federal Highway Administration (FHWA) Exploratory Advanced Research (693JJ323C000010) and the Texas A&M Institute Career Initiation Fellow Award.

Appendix 1:. Cayley-Hamilton Theorem

Theorem1. A is a given $n \times n$ matrix, and I_n is $n \times n$ identity matrix. Considering A with characteristic polynomial $p_A(\lambda) = \det(\lambda I_n - A) = \lambda^n + c_{n-1}\lambda^{n-1} + \cdots + c_0$, then $p_A(A) \equiv O_n$. The O_n is $n \times n$ null matrix. λ is an eigenvalue of A only when normal characteristic polynomial $p_A(\lambda) = 0$. Then, the Taylor-series expansion can be re-illustrated without truncation as follows:

$$e^{At} = \sum_{k=0}^{n-1} \alpha_k A^k \tag{A1}$$

where the α_k's are determined from the set of equations given by the eigenvalues of A.

$$e^{\lambda_i t} = \sum_{k=0}^{n-1} \alpha_k \lambda_i^k \tag{A2}$$

Appendix 2:. Proof of Proposition 1 and Proposition 2

The eigenvalues for A_d can be computed as:

$$\lambda^2 + (\tau^* k_s + k_v)\lambda + k_s = 0 \tag{A3}$$

By solving Eq.(A3), we can get A_d's eigenvalues λ_1 and λ_2 as:

$$\lambda_1 = \frac{-(\tau^* k_s + k_v) + \sqrt{(\tau^* k_s + k_v)^2 - 4k_s}}{2} \tag{A4}$$

$$\lambda_2 = \frac{-(\tau^* k_s + k_v) - \sqrt{(\tau^* k_s + k_v)^2 - 4k_s}}{2} \tag{A5}$$

From Eq. (A4) and (A5), we can find that, when $(\tau^* k_{si} + k_{vi})^2 - 4k_{si} \geq 0$, both λ_1 and λ_2 are real, α_k could be solved as below:

$$\begin{cases} e^{\lambda_1 t} = \alpha_0 + \alpha_1 \lambda_1 \\ e^{\lambda_2 t} = \alpha_0 + \alpha_1 \lambda_2 \end{cases} \Rightarrow \begin{cases} \alpha_0 = e^{\lambda_1 t} - \dfrac{e^{\lambda_1 t} - e^{\lambda_2 t}}{\lambda_1 - \lambda_2}\lambda_1 \\ \alpha_1 = \dfrac{e^{\lambda_1 t} - e^{\lambda_2 t}}{\lambda_1 - \lambda_2} \end{cases} \tag{A6}$$

By using Eq. (A1), we can obtain $e^{A_d t}$ with only real eigenvalues of A_d as Proposition 1.

By Eq. (A3), when $(\tau^* k_s + k_v)^2 - 4k_s < 0$, the eigenvalues are complex conjugate numbers, which further represent them as $\lambda_1 = z + yi$ and $\lambda_2 = z - yi$. According to Euler's formula $e^{ix} = \cos x + i\sin x$, we have $e^{\lambda_1 t} = e^{zt}(\cos yt + i\sin yt)$ and $e^{\lambda_2 t} = e^{zt}(\cos yt - i\sin yt)$. By solving Eq. (A2), we have:

$$\alpha_0 = e^{zt}(\cos yt - \frac{z}{y}\sin yt) \tag{A7}$$

$$\alpha_1 = \frac{e^{zt}}{y}\sin yt \tag{A8}$$

Appendix 3:. Proof of Lemma 1

Based on Proposition 3 and Eq. (7) under **Scenario 1**, Eq. (9-b) can be simplified as below:

$$At^2 + Bt + C = 0 \tag{A9}$$

When quadratic function Eq. (A9) has a positive solution, the ACC exhibit nonlinear behavior due to the bounded acceleration/deceleration, and the nonlinearity interval is $T_w = [\max\left(0, \min\left(\frac{-B \pm \sqrt{D}}{2A}\right)\right), \max(0, \max\left(\frac{-B \pm \sqrt{D}}{2A}\right))]$. Otherwise, the ACC follows linear control law. Furthermore, the ACC system exhibits a purely free response under **Scenario 1**, indicating that the bounded acceleration/deceleration can only occur to attenuate the impact of the initial cut-in condition so that the nonlinearity interval is revised as $T_w = [0, \max(0, \max\left(\frac{-B \pm \sqrt{D}}{2A}\right))]$. Therefore, Lemma 1 is derived.

Appendix 4:. Proof of Proposition 6

From Eq. (17), the spacing response in $[0, t_w]$ is the same as Eq. (13), and the extremum of it is $t^*_{\Delta d,n} = \frac{\Delta v_i(0) - u_b \tau^*}{u_b}$. The spacing response in (t_w, ∞) can be given as:

$$\Delta d_i(t) = e^{z(t-t_w)}\cos y(t-t_w)\Delta d_i(0) - \frac{e^{z(t-t_w)}(\tau^* k_s - z)}{y}\sin y(t-t_w)\Delta d_i(0) + \frac{e^{z(t-t_w)}(1-\tau^* k_v)}{y}\sin y(t-t_w)\Delta v_i(0) \tag{A10}$$

The solution of the derivative of Eq. (A10) for t is:

$$t^*_{\Delta d,l} = \frac{(2n+1)\pi + 2\arctan(B/A)}{2y} + t_w, n \in \mathbb{Z} \tag{A11}$$

Where, $A = z\Delta d_i(t_w) - \tau^* k_s \Delta d_i(t_w) + z\Delta d_i(t_w) + (1-\tau^* k_v)\Delta v_i(t_w)$ and $B = -y\Delta d_i(t_w) - \frac{z(\tau^* k_s - z)}{y}\Delta d_i(t_w) + \frac{z(1-\tau^* k_v)}{y}\Delta v_i(t_w)$.
By analyzing the time of extremum spacing response $\Delta d_i(t)$ and the corresponding extremum value, Proposition 6 can be obtained.

Appendix 5:. Proof of Proposition 7

Refer to Eq. (17) and Eq. (16-a), we have:

$$d_i(t) = \begin{cases} -\frac{u_b t^2}{2} + \Delta v_i(0)t + \tau^* v_{i-1}(t) + \Delta d_i(0) - \tau^* \Delta v_i(0) t \in [0, t_w] \\ e^{z(t-t_w)}\cos y(t-t_w)\Delta d_i(t_w) - \frac{e^{z(t-t_w)}(\tau^* k_s - z)}{y}\sin y(t-t_w)\Delta d_i(t_w) + \frac{e^{z(t-t_w)}(1-\tau^* k_v)}{y}\sin y(t-t_w)\Delta v_i(t_w) + v_{i-1}(t)\tau^* + \\ \frac{k_s e^{z(t-t_w)}}{y}\sin y(t-t_w)\tau^* \Delta d_i(t_w) - e^{z(t-t_w)}\cos y(t-t_w)\tau^* \Delta v_i(t_w) + \frac{e^{z(t-t_w)}(k_v - z)}{y}\sin y(t-t_w)\tau^* \Delta v_i(t_w) t \in (t_w, \infty) \end{cases} \tag{A12}$$

Then, Eq. (A12) can be simplified as Eq. (A13) and derivative it with respect to t, as in Eq. (A14).

$$d_i(t) = \begin{cases} -\frac{u_b t^2}{2} + \Delta v_i(0)t + \tau^* v_{i-1}(0) + \Delta d_i(0) - \tau^* \Delta v_i(0) t \in [0, t_w] \\ Ae^{zt}\cos y(t-t_w) + Be^{zt}\sin y(t-t_w) + Ct \in (t_w, \infty) \end{cases} \tag{A13}$$

$$\begin{cases} t^*_{d,n} = \frac{\Delta v_i(0)}{u_b} \\ t^*_{d,l} = \frac{(2n+1)\pi + 2\arctan(BZ - Ay/Az + By)}{2y} + t_w, n \in Z \end{cases} \tag{A14}$$

$$A = \Delta d_i(t_w) - \tau^* \Delta v_i(t_w); B = \frac{1}{y}(z\Delta d_i(t_w) + \Delta v_i(t_w) - z\tau^* \Delta v_i(t_w)); C = v_{i-1}(0)\tau^*$$

Appendix 6:. Derivation of Scenario 2 under oscillatory system

When Proposition 2 holds, the ACC dynamic evolution can be derived from Eqs. (4), (6), and (10) as Eq. (A15).

$$\begin{bmatrix} \Delta d_i(t) \\ \Delta v_i(t) \end{bmatrix} = \begin{cases} \begin{bmatrix} 1 & t \\ 0 & 1 \end{bmatrix}\begin{bmatrix} \Delta d_i(0) \\ \Delta v_i(0) \end{bmatrix} + \begin{bmatrix} -\frac{t^2}{2} - \tau^* t \\ -t \end{bmatrix} u_b + a_1 \begin{bmatrix} \frac{t^2}{2} \\ t \end{bmatrix} t \in [0, t_w] \\ \widetilde{\mathscr{M}}(t, t_w)\begin{bmatrix} \Delta d_i(t_w) \\ \Delta v_i(t_w) \end{bmatrix} + a_1 \widetilde{\mathscr{F}}(t, t_w) t \in (t_w, t_1] \\ \widetilde{\mathscr{M}}(t, t_1)\begin{bmatrix} \Delta d_i(t_1) \\ \Delta v_i(t_1) \end{bmatrix} + a_2 \widetilde{\mathscr{F}}(t, t_1) t \in (t_1, t_2] \\ \widetilde{\mathscr{M}}(t, t_2)\begin{bmatrix} \Delta d_i(t_2) \\ \Delta v_i(t_2) \end{bmatrix} t \in (t_2, \infty) \end{cases} \tag{A15}$$

Where $\widetilde{\mathscr{F}}(t, t_0) = \begin{bmatrix} \frac{(1-\tau^* k_v)}{y} \bullet \frac{y - e^{z(t-t_0)}(y\cos y(t-t_0) - z\sin y(t-t_0))}{y^2 + z^2} \\ \frac{e^{z(t-t_0)}(z\cos y(t-t_0) + y\sin y(t-t_0)) - z}{y^2 + z^2} + \frac{(k_v - z)}{y} \bullet \frac{e^{z(t-t_0)}(y\cos y(t-t_0) - z\sin y(t-t_0)) - y}{y^2 + z^2} \end{bmatrix}$ represents the function of forced response under oscillatory ACC system.

The derivation of the conditions for overshoot and safety aligns with the procedures outlined in Lemma 5 and 6. However, the functions of free and forced responses, as detailed in Eqs. (17) and (A15), are distinct for oscillatory and non-oscillatory ACC systems.

Appendix 7:. Dynamic Evolution of non-oscillatory ACC under Oscillation

In a more generic scenario, when oscillation $a_{i-1}(t) = M\sin wt$ is considered under a non-oscillatory ACC system, the state evolution of the ACC can be derived from Eqs. (4) and (5). Provided that the magnitude of oscillation remains within the acceleration/deceleration boundary, the non-linear behavior of the ACC system is primarily induced by the initial cut-in disturbance and the state evolution is adheres to Eq. (11) for $t \in [0, t_w]$. Besides, the state evolution of ACC following linear control law (i.e., $t \in (t_w, \infty)$) is derived as follows:

$$\begin{aligned}\begin{bmatrix}\Delta d_i(t)\\ \Delta v_i(t)\end{bmatrix} &= e^{A_d(t-t_0)}x_i(t_w) + \int_{t_0}^{t} e^{A_d(t-\varphi)}D_d a_{i-1}(\varphi)d\varphi\\ &= \begin{bmatrix} e^{\lambda_1(t-t_w)} - \dfrac{e^{\lambda_1(t-t_w)}-e^{\lambda_2(t-t_w)}}{\lambda_1-\lambda_2}(\lambda_1+\tau^* k_{si}) & \dfrac{e^{\lambda_1(t-t_w)}-e^{\lambda_2(t-t_w)}}{\lambda_1-\lambda_2}(1-\tau^* k_{vi})\\ -\dfrac{e^{\lambda_1(t-t_w)}-e^{\lambda_2(t-t_w)}}{\lambda_1-\lambda_2}k_{si} & e^{\lambda_1(t-t_0)} - \dfrac{e^{\lambda_1(t-t_w)}-e^{\lambda_2(t-t_w)}}{\lambda_1-\lambda_2}(\lambda_1+k_{vi})\end{bmatrix}\begin{bmatrix}\Delta d_i(t_w)\\ \Delta v_i(t_w)\end{bmatrix}\\ &+ \begin{bmatrix} \dfrac{(1-\tau^* k_{vi})e^{\lambda_1 t}}{\lambda_1-\lambda_2}\displaystyle\int_{t_w}^{t} e^{-\lambda_1\varphi}a_{i-1}(\varphi)d\varphi - \dfrac{(1-\tau^* k_{vi})e^{\lambda_2 t}}{\lambda_1-\lambda_2}\int_{t_w}^{t} e^{-\lambda_2\varphi}a_{i-1}(\varphi)d\varphi\\ e^{\lambda_1 t}\displaystyle\int_{t_w}^{t} e^{-\lambda_1\varphi}a_{i-1}(\varphi)d\varphi - \dfrac{(\lambda_1+k_{vi})e^{\lambda_1 t}}{\lambda_1-\lambda_2}\int_{t_w}^{t} e^{-\lambda_1\varphi}a_{i-1}(\varphi)d\varphi - \dfrac{(\lambda_1+k_{vi})e^{\lambda_2 t}}{\lambda_1-\lambda_2}\int_{t_w}^{t} e^{-\lambda_2\varphi}a_{i-1}(\varphi)d\varphi\end{bmatrix}\end{aligned} \tag{A16}$$

By substituting $a_{i-1}(\varphi) = M\sin w\varphi$ into Eq. (A16) and find integral of φ, we have Eq. (A17).

$$\begin{bmatrix}\Delta d_i(t)\\ \Delta v_i(t)\end{bmatrix} = \begin{cases}\begin{bmatrix}1 & t\\ 0 & 1\end{bmatrix}\begin{bmatrix}\Delta d_i(0)\\ \Delta v_i(0)\end{bmatrix} + \begin{bmatrix}-\dfrac{t^2}{2} - \tau^* t\\ -t\end{bmatrix} u_b t \in [0, t_w]\\ M(t, t_w)\begin{bmatrix}\Delta d_i(t_w)\\ \Delta v_i(t_w)\end{bmatrix} + MH(t, t_w) t \in (t_w, \infty)\end{cases} \tag{A17}$$

where

$$\mathscr{M}(t, t_w) = \begin{bmatrix} e^{\lambda_1(t-t_w)} - \dfrac{e^{\lambda_1(t-t_w)}-e^{\lambda_2(t-t_w)}}{\lambda_1-\lambda_2}(\lambda_1+\tau^* k_{si}) & \dfrac{e^{\lambda_1(t-t_w)}-e^{\lambda_2(t-t_w)}}{\lambda_1-\lambda_2}(1-\tau^* k_{vi})\\ -\dfrac{e^{\lambda_1(t-t_w)}-e^{\lambda_2(t-t_w)}}{\lambda_1-\lambda_2}k_{si} & e^{\lambda_1(t-t_0)} - \dfrac{e^{\lambda_1(t-t_w)}-e^{\lambda_2(t-t_w)}}{\lambda_1-\lambda_2}(\lambda_1+k_{vi})\end{bmatrix}$$

and

$$\mathscr{H}(t, t_w) = \begin{bmatrix} \dfrac{(1-\tau^* k_{vi})e^{\lambda_1 t}}{\lambda_1-\lambda_2}\left(\dfrac{e^{-\lambda_1 t_w}(w\cos wt_w + \lambda_1{}^*\sin wt_w) - e^{-\lambda_1 t}(w\cos wt + \lambda_1{}^*\sin wt)}{\lambda_1 + w^2}\right)\\ -\dfrac{(1-\tau^* k_{vi})e^{\lambda_2 t}}{\lambda_1-\lambda_2}\left(\dfrac{e^{-\lambda_2 t_w}(w\cos wt_w + \lambda_2{}^*\sin wt_w) - e^{-\lambda_2 t}(w\cos wt + \lambda_2{}^*\sin wt)}{\lambda_2 + w^2}\right)\\ \dfrac{M(-\lambda_2 - k_{vi})e^{\lambda_1 t}}{\lambda_1-\lambda_2}\left(\dfrac{e^{-\lambda_1 t_w}(w\cos wt_w + \lambda_1{}^*\sin wt_w) - e^{-\lambda_1 t}(w\cos wt + \lambda_1{}^*\sin wt)}{\lambda_1 + w^2}\right)\\ -\dfrac{(\lambda_1+k_{vi})e^{\lambda_2 t}}{\lambda_1-\lambda_2}\left(\dfrac{e^{-\lambda_2 t_w}(w\cos wt_w + \lambda_2{}^*\sin wt_w) - e^{-\lambda_2 t}(w\cos wt + \lambda_2{}^*\sin wt)}{\lambda_2 + w^2}\right)\end{bmatrix}.$$

References

Ahn, S., Cassidy, M.J., 2007. Freeway traffic oscillations and vehicle lane-change maneuvers, in: Transportation and Traffic Theory 2007. Papers Selected for Presentation at ISTTT17Engineering and Physical Sciences Research Council (Great Britain) Rees Jeffreys Road FundTransport Research FoundationTMS ConsultancyOve Arup and Partners, Hong KongTransportation Planning (International) PTV AG.

Bang, S., Ahn, S., 2018. Control of connected and autonomous vehicles with cut-in movement using spring mass damper system. Transp. Res. Rec. 2672, 133–143. https://doi.org/10.1177/0361198118796927.

Brunner, J.S., Makridis, M.A., Kouvelas, A., 2022. Comparing the observable response times of ACC and CACC systems. IEEE Trans. Intell. Transp. Syst. 23, 19299–19308. https://doi.org/10.1109/TITS.2022.3165648.

Chen, D., Srivastava, A., Ahn, S., Li, T., 2020. Traffic dynamics under speed disturbance in mixed traffic with automated and non-automated vehicles. Transportation Research Part C: Emerging Technologies, ISTTT 23 TR_C-23rd International Symposium on Transportation and Traffic Theory (ISTTT 23) 113, 293–313. Doi: 10.1016/j.trc.2019.03.017.

Chen, K., Knoop, V.L., Liu, P., Li, Z., Wang, Y., 2023. Modeling the impact of lane-changing's anticipation on car-following behavior. Transportation Research Part c: Emerging Technologies 150, 104110. https://doi.org/10.1016/j.trc.2023.104110.

Chen, T., Wang, M., Gong, S., Zhou, Y., Ran, B., 2021. Connected and automated vehicle distributed control for on-ramp merging scenario: a virtual rotation approach. Transportation Research Part c: Emerging Technologies 133, 103451.

Cheng, R., Orosz, G., Murray, R.M., Burdick, J.W., 2019. End-to-end safe reinforcement learning through barrier functions for safety-critical continuous control tasks. In: Proceedings of the AAAI Conference on Artificial Intelligence, pp. 3387–3395.

Franklin, G.F., Powell, J.D., Emami-Naeini, A., Powell, J.D., 2002. Feedback control of dynamic systems. Prentice Hall Upper Saddle River.

Gunter, G., Gloudemans, D., Stern, R.E., McQuade, S., Bhadani, R., Bunting, M., Delle Monache, M.L., Lysecky, R., Seibold, B., Sprinkle, J., Piccoli, B., Work, D.B., 2021. Are Commercially implemented adaptive cruise control systems string stable? IEEE Trans. Intell. Transp. Syst. 22, 6992–7003. https://doi.org/10.1109/TITS.2020.3000682.

Jayasuriya, S., Dharne, A.G., 2002. Necessary and sufficient conditions for non-overshooting step responses for LTI systems, in: Proceedings of the 2002 American Control Conference (IEEE Cat. No.CH37301). Presented at the Proceedings of the 2002 American Control Conference (IEEE Cat. No.CH37301), pp. 505–510 vol.1. Doi: 10.1109/ACC.2002.1024856.

Jiang, J., Zhou, Y., Wang, X., Ahn, S., 2023. A generic stochastic hybrid Car-following model based on approximate bayesian computation. Transportation Research Board 102nd Annual Meeting..

Kazemi, H., Mahjoub, H.N., Tahmasbi-Sarvestani, A., Fallah, Y.P., 2018. A learning-based stochastic MPC design for cooperative adaptive cruise control to handle interfering vehicles. IEEE Trans. Intell. Veh. 3, 266–275.

Khound, P., Will, P., Gronwald, F., 2021. Design methodology to derive over-damped string stable adaptive cruise control systems. IEEE Trans. Intell. Veh. 7, 32–44.

Knoop, V.L., Wang, M., Wilmink, I., Hoedemaeker, D.M., Maaskant, M., Van der Meer, E.-J., 2019. Platoon of SAE Level-2 automated vehicles on public roads: setup, traffic Interactions, and stability. Transp. Res. Rec. 2673, 311–322. https://doi.org/10.1177/0361198119845885.

Li, X., 2022. Trade-off between safety, mobility and stability in automated vehicle following control: an analytical method. Transp. Res. B Methodol. 166, 1–18. https://doi.org/10.1016/j.trb.2022.09.003.

Li, T., Chen, D., Zhou, H., Laval, J., Xie, Y., 2021. Car-following behavior characteristics of adaptive cruise control vehicles based on empirical experiments. Transp. Res. B Methodol. 147, 67–91. https://doi.org/10.1016/j.trb.2021.03.003.

Li, T., Chen, D., Zhou, H., Xie, Y., Laval, J., 2022. Fundamental diagrams of commercial adaptive cruise control: worldwide experimental evidence. Transportation Research Part c: Emerging Technologies 134, 103458. https://doi.org/10.1016/j.trc.2021.103458.

Li, Z., Zhou, Y., Zhang, Y., Li, X., 2023. Enhancing Vehicular Platoon Stability in the Presence of Communication Cyberattacks: A Reliable Longitudinal Cooperative Control Strategy. Available at SSRN 4633758.

Li, Y., Li, Z., Wang, H., Wang, W., Xing, L., 2017. Evaluating the safety impact of adaptive cruise control in traffic oscillations on freeways. Accid. Anal. Prev. 104, 137–145.

Li, P.Y., Shrivastava, A., 2002. Traffic flow stability induced by constant time headway policy for adaptive cruise control vehicles. Transportation Research Part c: Emerging Technologies 10, 275–301. https://doi.org/10.1016/S0968-090X(02)00004-9.

Liu, X., Goldsmith, A., Mahal, S.S., Hedrick, J.K., 2001. Effects of communication delay on string stability in vehicle platoons, in: ITSC 2001. 2001 IEEE Intelligent Transportation Systems. Proceedings (Cat. No. 01TH8585). IEEE, pp. 625–630.

Makridis, M., Mattas, K., Anesiadou, A., Ciuffo, B., 2021. OpenACC. an open database of car-following experiments to study the properties of commercial ACC systems. Transportation Research Part c: Emerging Technologies 125, 103047. https://doi.org/10.1016/j.trc.2021.103047.

Marsden, G., McDonald, M., Brackstone, M., 2001. Towards an understanding of adaptive cruise control. Transportation Research Part c: Emerging Technologies 9, 33–51. https://doi.org/10.1016/S0968-090X(00)00022-X.

Milanés, V., Shladover, S.E., 2016. Handling cut-in vehicles in strings of cooperative adaptive cruise control vehicles. J. Intell. Transp. Syst. 20, 178–191.

Montanino, M., Punzo, V., 2021. On string stability of a mixed and heterogeneous traffic flow: a unifying modelling framework. Transp. Res. B Methodol. 144, 133–154. https://doi.org/10.1016/j.trb.2020.11.009.

Naus, G.J., Vugts, R.P., Ploeg, J., van De Molengraft, M.J., Steinbuch, M., 2010. String-stable CACC design and experimental validation: a frequency-domain approach. IEEE Trans. Veh. Technol. 59, 4268–4279.

Nise, N.S., 2020. Control systems engineering. John Wiley & Sons.

Orosz, G., 2016. Connected cruise control: modelling, delay effects, and nonlinear behaviour. Veh. Syst. Dyn. 54, 1147–1176. https://doi.org/10.1080/00423114.2016.1193209.

Ossen, S., Hoogendoorn, S.P., 2011. Heterogeneity in car-following behavior: theory and empirics. Transportation Research Part c: Emerging Technologies, Emerging Theories in Traffic and Transportation and Methods for Transportation Planning and Operations 19, 182–195. https://doi.org/10.1016/j.trc.2010.05.006.

Ploeg, J., van de Wouw, N., Nijmeijer, H., 2014. Lp string stability of cascaded systems: application to vehicle platooning. IEEE Trans. Control Syst. Technol. 22, 786–793. https://doi.org/10.1109/TCST.2013.2258346.

Sharma, A., Zheng, Z., Bhaskar, A., 2019. Is more always better? the impact of vehicular trajectory completeness on car-following model calibration and validation. Transp. Res. B Methodol. 120, 49–75.

Shi, X., Li, X., 2021. Empirical study on car-following characteristics of commercial automated vehicles with different headway settings. Transportation Research Part c: Emerging Technologies 128, 103134.

Shi, H., Zhou, Y., Wu, K., Wang, X., Lin, Y., Ran, B., 2021. Connected automated vehicle cooperative control with a deep reinforcement learning approach in a mixed traffic environment. Transportation Research Part c: Emerging Technologies 133, 103421. https://doi.org/10.1016/j.trc.2021.103421.

Straubing, H., 1983. A combinatorial proof of the cayley-Hamilton theorem. Discret. Math. 43, 273–279.

Treiber, M., Kesting, A., Helbing, D., 2006. Delays, inaccuracies and anticipation in microscopic traffic models. Physica A 360, 71–88. https://doi.org/10.1016/j.physa.2005.05.001.

van Arem, B., van Driel, C.J.G., Visser, R., 2006. The impact of cooperative adaptive cruise control on traffic-flow Characteristics. IEEE Trans. Intell. Transp. Syst. 7, 429–436. https://doi.org/10.1109/TITS.2006.884615.

Wang, C., Gong, S., Zhou, A., Li, T., Peeta, S., 2020. Cooperative adaptive cruise control for connected autonomous vehicles by factoring communication-related constraints. Transportation Research Part C: Emerging Technologies, ISTTT 23 TR_C-23rd International Symposium on Transportation and Traffic Theory (ISTTT 23) 113, 124–145. Doi: 10.1016/j.trc.2019.04.010.

Wang, M., Hoogendoorn, S.P., Daamen, W., van Arem, B., Happee, R., 2015. Game theoretic approach for predictive lane-changing and car-following control. Transportation Research Part c: Emerging Technologies 58, 73–92. https://doi.org/10.1016/j.trc.2015.07.009.

Wang, Y., Li, X., Tian, J., Jiang, R., 2020b. Stability analysis of stochastic linear car-following models. Transp. Sci. 54, 274–297.

Ward, J.A., 2009. Heterogeneity, lane-changing and instability in traffic: A mathematical approach.

Zhang, L., Sun, J., Orosz, G., 2018. Hierarchical Design of Connected Cruise Control in the presence of information delays and uncertain vehicle dynamics. IEEE Trans. Control Syst. Technol. 26, 139–150. https://doi.org/10.1109/TCST.2017.2664721.

Zhao, C., Wang, W., Li, S., Gong, J., 2019. Influence of cut-in maneuvers for an autonomous car on surrounding drivers: experiment and analysis. IEEE Trans. Intell. Transp. Syst. 21, 2266–2276.

Zheng, Z., Ahn, S., Monsere, C.M., 2010. Impact of traffic oscillations on freeway crash occurrences. Accid. Anal. Prev. 42, 626–636. https://doi.org/10.1016/j.aap.2009.10.009.

Zheng, Z., Ahn, S., Chen, D., Laval, J., 2013. The effects of lane-changing on the immediate follower: anticipation, relaxation, and change in driver characteristics. Transportation Research Part c: Emerging Technologies 26, 367–379. https://doi.org/10.1016/j.trc.2012.10.007.

Zhou, Y., Ahn, S., Chitturi, M., Noyce, D.A., 2017. Rolling horizon stochastic optimal control strategy for ACC and CACC under uncertainty. Transportation Research Part c: Emerging Technologies 83, 61–76. https://doi.org/10.1016/j.trc.2017.07.011.

Zhou, Y., Wang, M., Ahn, S., 2019. Distributed model predictive control approach for cooperative car-following with guaranteed local and string stability. Transp. Res. B Methodol. 128, 69–86. https://doi.org/10.1016/j.trb.2019.07.001.

Zhou, Y., Jafarsalehi, G., Jiang, J., Wang, X., Ahn, S., Lee, J.D., 2022b. Stochastic calibration of automated vehicle Car-following control. An Approximate Bayesian Computation Approach. Available at SSRN 4084970.

Zhou, H., Zhou, A., Li, T., Chen, D., Peeta, S., Laval, J., 2022a. Significance of low-level control to string stability under adaptive cruise control: algorithms, theory and experiments. Transportation Research Part c: Emerging Technologies 140, 103697. https://doi.org/10.1016/j.trc.2022.103697.